Nit1 is a metabolite repair enzyme that hydrolyzes deaminated glutathione

Alessio Peracchi[a,b,c,1,2,3,4], Maria Veiga-da-Cunha[a,b,3,4], Tomiko Kuhara[d,e], Kenneth W. Ellens[f], Nicole Paczia[f], Vincent Stroobant[g], Agnieszka K. Seliga[a,b], Simon Marlaire[a,b], Stephane Jaisson[a,b,5], Guido T. Bommer[a,b], Jin Sun[h], Kay Huebner[h], Carole L. Linster[f], Arthur J. L. Cooper[i], and Emile Van Schaftingen[a,b,4]

[a]Walloon Excellence in Lifesciences and Biotechnology, B-1200 Brussels, Belgium; [b]de Duve Institute, Université Catholique de Louvain, B-1200 Brussels, Belgium; [c]Department of Life Sciences, Laboratory of Biochemistry, Molecular Biology, and Bioinformatics, University of Parma, 43124 Parma, Italy; [d]Japan Clinical Metabolomics Institute, Kahoku, Ishikawa 929-1174, Japan; [e]Human Genetics, Medical Research Institute, Kanazawa Medical University, Uchinada, Ishikawa 920-0293, Japan; [f]Luxembourg Centre for Systems Biomedicine, Université du Luxembourg, L-4367 Belvaux, Luxembourg; [g]Ludwig Institute for Cancer Research, de Duve Institute, Université Catholique de Louvain, B-1200 Brussels, Belgium; [h]Department of Cancer Biology and Genetics, Ohio State University, Columbus, OH 43210; and [i]Department of Biochemistry and Molecular Biology, New York Medical College, Valhalla, NY 10595

Edited by Shelley D. Copley, University of Colorado, Boulder, CO, and accepted by Editorial Board Member Stephen J. Benkovic March 9, 2017 (received for review August 17, 2016)

The mammalian gene *Nit1* (nitrilase-like protein 1) encodes a protein that is highly conserved in eukaryotes and is thought to act as a tumor suppressor. Despite being ∼35% sequence identical to ω-amidase (Nit2), the Nit1 protein does not hydrolyze efficiently α-ketoglutaramate (a known physiological substrate of Nit2), and its actual enzymatic function has so far remained a puzzle. In the present study, we demonstrate that both the mammalian Nit1 and its yeast ortholog are amidases highly active toward deaminated glutathione (dGSH; i.e., a form of glutathione in which the free amino group has been replaced by a carbonyl group). We further show that *Nit1*-KO mutants of both human and yeast cells accumulate dGSH and the same compound is excreted in large amounts in the urine of *Nit1*-KO mice. Finally, we show that several mammalian aminotransferases (transaminases), both cytosolic and mitochondrial, can form dGSH via a common (if slow) side-reaction and provide indirect evidence that transaminases are mainly responsible for dGSH formation in cultured mammalian cells. Altogether, these findings delineate a typical instance of metabolite repair, whereby the promiscuous activity of some abundant enzymes of primary metabolism leads to the formation of a useless and potentially harmful compound, which needs a suitable "repair enzyme" to be destroyed or reconverted into a useful metabolite. The need for a dGSH repair reaction does not appear to be limited to eukaryotes: We demonstrate that Nit1 homologs acting as excellent dGSH amidases also occur in *Escherichia coli* and other glutathione-producing bacteria.

metabolite repair | deaminated glutathione | amidase | aminotransferases

Genome sequencing has led to the identification of numerous proteins sharing significant sequence identity with enzymes, but whose catalytic activity remains to be established. Knowing the function of these putative enzymes, particularly if they are highly conserved, may reveal important aspects of intermediary metabolism that have remained unexplored until now. The purpose of the present work was to determine the catalytic role of nitrilase-like protein 1 (Nit1), a highly conserved protein with still unknown function (1–6) but homologous to Nit2 (ω-amidase) (5, 6), an enzyme whose activity is closely linked to transamination reactions.

In fact, aminotransferases that use L-glutamine as a substrate yield, as a product, the corresponding ketoacid, α-ketoglutaramate (α-KGM) (Fig. 1*A*). Such a reaction is rendered metabolically irreversible by the coupled activity of ω-amidase, which hydrolyzes α-KGM to α-ketoglutarate (α-KG) and ammonia (Fig. 1*A*) (7–9). In mammals, ω-amidase is encoded by the *Nit2* gene (5, 6).

In addition to *Nit2*, the genomes of the most evolved eukaryotes contain almost invariably the gene *Nit1*, whose product shows ∼35% sequence identity with Nit2. Compared with Nit2, however, the Nit1 protein shows only weak ω-amidase activity toward α-KGM (catalytic efficiency <0.1% of that of Nit2) (5). The observation that in many invertebrates Nit1 is expressed as a domain fused with a fragile histidine triad protein (Fhit, suggested to act as a tumor suppressor in mammals) (1), has fueled a substantial interest in deciphering the physiological substrates of this enzyme. Galperin and Koonin even included *Nit1* among the "top 10" most attractive targets for functional assignment (10, 11), assuming that clarification of its activity could illuminate new aspects of biology. Despite all this interest, the actual enzymatic function of Nit1 has so far remained elusive.

Sequence comparisons and structural data indicate that the residues of the Nit2 catalytic pocket that surround the substrate α-KGM are conserved in Nit1. A major difference is, however,

Significance

The genomes of the vast majority of eukaryotes encode a protein [named nitrilase-like protein 1 (Nit1) in humans and mice] whose enzymatic function has long been unknown. We show here that the mammalian Nit1 and the corresponding yeast protein efficiently hydrolyze the deaminated form of the common intracellular antioxidant glutathione. In turn, deaminated glutathione can be produced by a side activity of numerous transaminases. Thus, Nit1 repairs an undesired product, arising from the slow (and erroneous) transformation of an important metabolite by some abundant intracellular enzymes. The importance of this Nit1 function is underscored by the finding that enzymes with the same activity occur in *Escherichia coli* and in other glutathione-producing bacteria.

Author contributions: A.P., M.V.-d.-C., and E.V.S. designed research; A.P., M.V.-d.-C., T.K., K.W.E., N.P., V.S., A.K.S., S.M., S.J., G.T.B., and C.L.L. performed research; J.S. and K.H. contributed new reagents/analytic tools; A.P., M.V.-d.-C., T.K., K.W.E., N.P., V.S., A.K.S., S.M., S.J., G.T.B., C.L.L., A.J.L.C., and E.V.S. analyzed data; and A.P. and E.V.S. wrote the paper.

The authors declare no conflict of interest.

This article is a PNAS Direct Submission. S.D.C. is a guest editor invited by the Editorial Board.

Freely available online through the PNAS open access option.

[1]A.P. mainly contributed to the present research while on sabbatical leave at the de Duve Institute, Université Catholique de Louvain.

[2]Present address: Department of Chemistry, Life Sciences, and Environmental Sustainability, University of Parma, 43124 Parma, Italy.

[3]A.P. and M.V.-d.-C. contributed equally to this work.

[4]To whom correspondence may be addressed. Email: alessio.peracchi@unipr.it, maria.veiga@uclouvain.be, or emile.vanschaftingen@uclouvain.be.

[5]Present address: Laboratory of Paediatric Biology and Research, University Hospital of Reims, Maison Blanche Hospital, 51092 Reims, France.

This article contains supporting information online at www.pnas.org/lookup/suppl/doi:10.1073/pnas.1613736114/-/DCSupplemental.

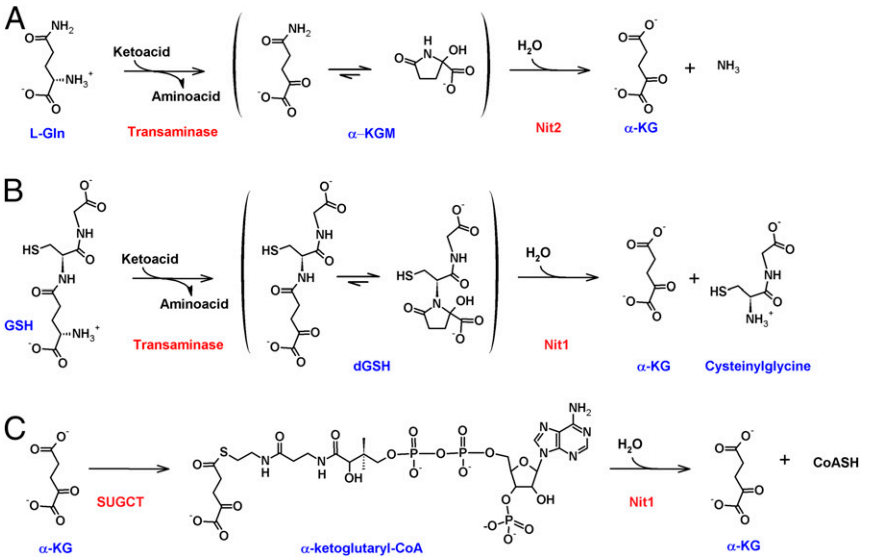

Fig. 1. The Nit2 reaction and the working hypotheses tested in this work about Nit1 activity. (*A*) The known coupled reactions catalyzed by glutamine transaminases and ω-amidase (Nit2). The transamination of glutamine yields α-KGM, the linear form of which equilibrates with a cyclic form (two potential anomers). Nit2 catalyzes the hydrolysis of the open form to α-KG and ammonia. (*B*) An analogous process, in which the transamination of GSH to dGSH is followed by hydrolysis of dGSH to α-KG and cysteinylglycine. (*C*) α-KG–CoA, formed by SUGCT (C7orf10), is another potential substrate for Nit1.

found in the subsite where the amido group of α-KGM is predicted to bind, which is a quite small niche in the structure of Nit2, but a much larger cavity in Nit1 (2, 4). These structural features suggest that Nit1 serves to hydrolyze an α-KG or α-KGM derivative attached to a rather large structure. Because no classic reaction of intermediary metabolism leads to the formation of such compounds, we considered the possibility that nonclassic compounds could be formed by side reactions of classic enzymes of intermediary metabolism and that Nit1 would serve as a "metabolite repair" enzyme.

Recent research has unveiled the importance of metabolite repair in intermediary metabolism (12, 13). According to this concept, enzymes of intermediary metabolism are not perfectly specific and tend to act on intracellular compounds resembling their true substrate. The products of these side reactions are nonclassic metabolites, which in several cases need to be eliminated or recycled by specific enzymes, called metabolite repair enzymes (12). Deficiency in such enzymes causes accumulation of the "abnormal" metabolite and may lead to disease, as in the case of L-2-hydroxyglutaric aciduria (14, 15) or to major metabolic perturbations because of enzyme inhibition (16). The increasing rate at which repair enzymes are being discovered suggests that a substantial fraction of currently "unclassified" enzymes (17), encoded in eukaryotic and prokaryotic genomes, could play a role in metabolite repair.

Conceivably, at least two types of reactions might lead to the formation of bulky ω-derivatives of α-KG: (*i*) transamination reactions leading to the conversion of glutathione (GSH) to a deaminated form (called deaminated GSH or dGSH in the present work) (Fig. 1*B*); and (*ii*) the "erroneous" attachment of a CoA group to α-KG by succinyl-CoA:glutarate-CoA transferase (SUGCT), which would lead to α-ketoglutaryl–CoA (α-KG–CoA) (Fig. 1*C*). Our purpose was to test these compounds as substrates for Nit1. In this work, we provide evidence that mouse Nit1 (mmNit1) and its *Saccharomyces cerevisiae* ortholog (scNit1; see Table 1 for the designation of the proteins investigated in the present work) are excellent dGSH amidases and that their inactivation leads to the accumulation of dGSH in cell models as well as in vivo.

Results

Nit1 Efficiently Hydrolyzes the Amide Bond in dGSH. dGSH and deaminated ophthalmic acid (dOA)—OA is a physiological tripeptide analog of GSH where the central cysteine is replaced by 2-aminobutyrate, a cysteine structural analog unable to form disulfides—as well as α-KGM, were prepared by oxidation of the appropriate compounds with snake venom L-amino acid oxidase, an enzyme that displays broad specificity (18, 19), and subsequently separated from the parent compound by cation-exchange chromatography (5). When dGSH and dOA were further purified by reverse-phase HPLC, both compounds eluted in two

Table 1. Proteins investigated in the present work

Species	Gene reference (DOE website)	Gene symbol	Protein designation
Mus musculus	639390753	*Nit1*	mmNit1
	639398620	*Nit2*	mmNit2
Saccharomyces cerevisiae	638211686	*NIT2*	scNit1
	638212758	*NIT3*	scNit2
Escherichia coli	646917127	*ybeM (ybl23)*	ecYbeM
	646916767	*yafV*	ecYafV
Yersinia enterocolitica	2638510043	*y0194*	yeNit1
	2638509534	No gene symbol	yeYafV
Pseudomonas aeruginosa	2687301550	*PA4475*	paNit1
	2687297946	*PA3797*	paYafV
Synechocystis sp. *GT-S, PCC6803*	651080170	*sll0601*	syNit1
Bifidobacterium longum	2650840504	No gene symbol	blYbeM
Staphylococcus aureus	2511961111	*amiE*	saYafV

Genes and protein sequences can be retrieved from the Department of Energy (DOE) website (https://img.jgi.doe.gov/cgi-bin/mer/main.cgi). The designations for the bacterial proteins studied in this work other than *E. coli* have been chosen based on their degree of identity with the mouse or *E. coli* proteins (see *SI Appendix*, Fig. S14 and Table S3). For example, blYbeM shows a higher degree of identity with ecYbeM than with mmNit1, mmNit2, or ecYafV; similarly, paNit1 shows a higher degree of identity with mmNit1 than with mmNit2, ecYbeM or ecYafV.

different peaks, corresponding to the two anomeric forms of the cyclized ketoacid. A peak attributable to the linear form was not detectable, suggesting that, in analogy with the case of α-KGM (20), such a linear form is largely unfavored for dGSH and dOA. dGSH, in addition to the two anomeric peaks, presented additional peaks eluting later and corresponding to disulfides of dGSH with GSH and with itself. Such additional peaks disappeared if the sample was treated with excess DTT before chromatography.

After purification, dGSH and dOA were tested as substrates for the recombinant mouse enzymes (mmNit1 and mmNit2) and for their yeast homologs, using a coupled assay with glutamate dehydrogenase (GDH) that monitors the release of α-KG. As shown in Table 2 and its legend, both dGSH and dOA are good substrates for mmNit1 and scNit1, whereas α-KGM is a much poorer substrate. Conversely, mmNit2 and its yeast counterpart acted efficiently on the small substrate α-KGM but showed no detectable activity toward the larger substrates derived from GSH and OA.

Having established that the Nit1 activity releases α-KG from dGSH and dOA, we also tested whether the other products of these reactions are, respectively, cysteinylglycine and 2-aminobutyrylglycine, as expected. Generation of stoichiometric amounts of 2-aminobutyrylglycine from dOA was demonstrated by *N*-labeling the reaction mixture with 6-aminoquinolyl-*N*-hydroxysuccinimidyl carbamate (AQC) and identifying the AQC-derivative of the dipeptide by reverse-phase HPLC (*SI Appendix*, Fig. S1). For unknown reasons, we were unable to detect the second product of dGSH cleavage by this method, but could easily measure the formation of cysteinylglycine directly in the reaction mixture, exploiting its known propensity to form a thiazolidine adduct with pyridoxal 5′-phosphate (PLP) (21). Because the formation of this adduct requires the presence of both a free amino group and of a free thiol on the same molecule (21), this technique confirmed that cysteinylglycine was formed in stoichiometric amounts during dGSH cleavage (*SI Appendix*, Fig. S2).

It is well established that ω-amidase acts on the linear form of α-KGM (20), despite the fact that in solution this form is 300-fold less abundant than the cyclic (lactam) forms (Fig. 1*A*). Because substituted derivatives of α-KGM also tend to cyclize, we tested the effect of increasing mmNit1 concentrations on the rate of dGSH hydrolysis. The measured reaction rate leveled off at high enzyme concentration, implying that under those conditions opening of the cyclic form becomes rate-limiting for the whole process (*SI Appendix*, Fig. S3*A*). From this experiment, we inferred an apparent first-order rate constant for ring opening of 0.26 min^{-1} at pH 7.2. By comparison, at the same pH, opening of the α-KGM form occurs with an apparent first-order rate constant of 0.0011 min^{-1} (20). This difference is likely attributable to internal catalysis because of the presence of the thiol group and of the glycine carboxylic group in dGSH. Consistent with this interpretation, the corresponding opening of cyclic dOA appears to be about 10-fold slower compared with dGSH (*SI Appendix*, Fig. S3*B*).

With this information in hand, we designed experiments to measure the catalytic parameters exhibited by mmNit1 and its yeast ortholog (scNit1) under conditions where the opening of the cyclic form is not rate limiting. As shown in Table 2, the apparent catalytic efficiencies (k_{cat}/K_M) toward dGSH for mmNit1and scNit1 are in the range 10^4 to 10^5 $M^{-1}\cdot s^{-1}$, over 1,000-fold higher than those observed toward α-KGM. These apparent k_{cat}/K_M values are also close to the "average" value for metabolic enzymes (22). If one considers that the actual substrate of these amidases is in fact the (minimally abundant) linear form of dGSH, as shown above, the "correct" k_{cat}/K_M values for mmNit1 and its yeast counterpart should greatly exceed 10^6 $M^{-1}\cdot s^{-1}$.

dGSH Accumulates in *Nit1*-Deficient Model Cells and in the Urine of *Nit1*-KO Mice. We prepared human cell lines (HAP1) deficient in Nit1 and Nit2 by CrispR/Cas9 technology. We selected two distinct *Nit1*-KO clones, targeted at two locations of the *Nit1* gene by using different guide RNAs, as described in *Materials and Methods*. Sequencing of the DNA indicated the presence of mutations incompatible with the production of an active Nit1 protein in these clones (*SI Appendix*, *Supplementary Materials and Methods*). Analysis of cell extracts by liquid chromatography-mass spectrometry (LC/MS) indicated the presence of a peak with the same exact *m/z* ratio and elution volume as dGSH (*SI Appendix*, Fig. S4*A*). Analysis of samples derived from cells deficient in Nit2 or from control cells revealed much lower amounts of the same compound. Assuming a water cell volume of 2.5 μL/mg protein, we estimated that the intracellular dGSH

Table 2. Observed rates and catalytic parameters for the reactions catalyzed by recombinant mouse Nit1 and Nit2 and by their yeast orthologs

α-KGM or dGSH	Activity at 80 μM substrate (μmol·min^{-1}·mg^{-1})	V_{max}* (μmol· min^{-1}·mg^{-1})	k_{cat} (s^{-1})	K_M (μM)	k_{cat}/K_M ($M^{-1}\cdot s^{-1}$)
α-KGM					
mmNit1	$2.6 \times 10^{-3} \pm 3 \times 10^{-4}$	—	—	—	18 ± 2†
scNit1	$1.5 \times 10^{-3} \pm 2 \times 10^{-4}$	—	—	—	12 ± 2†
mmNit2	4.3 ± 0.5	19.4 ± 1.4	10.7 ± 0.7	250 ± 40	43,000 ± 3,000
scNit2	1.6 ± 0.23	40.2 ± 1.5	23.5 ± 0.9	1,600 ± 200	14,700 ± 2,100
dGSH					
mmNit1	0.8 ± 0.05	2.6 ± 0.4	1.6 ± 0.3	170 ± 60	9,400 ± 3,000
scNit1	2.7 ± 0.5	5.8 ± 0.5	3.6 ± 0.3	45 ± 6	80,000 ± 12,000
mmNit2	$\leq 3 \times 10^{-4}$	—	—	—	<3
scNit2	$\leq 1.6 \times 10^{-4}$	—	—	—	<2

Values are the average (± SEM) of at least three separate measurements. Activities were determined at pH 8.5 (30 °C) and at enzyme concentrations calibrated to ensure that the spontaneous opening of the cyclic forms of the substrates was not rate-limiting for the reaction measured. Details are provided in *Materials and Methods*. Activities (μmol·min^{-1}·mg^{-1}) toward 80 μM dOA were 0.07 ± 0.01 (mmNit1), 0.85 ± 0.03 (scNit1), $\leq 2 \times 10^{-4}$ (mmNit2) and $\leq 3 \times 10^{-4}$ (scNit2).

*Specific activity at saturating concentration of substrate.

†k_{cat}/K_M corresponds to the initial slope of the Michaelis-Menten hyperbola. Because the activities of both mmNit1 and scNit1 toward α-KGM increased linearly with substrate concentration up to at least 80 μM, k_{cat}/K_M values were estimated from the slopes of such increases. Because of the very low activity of mmNit1 and scNit1 with α-KGM, enzyme concentrations in these experiments were in the 0.5–1.5 μM range.

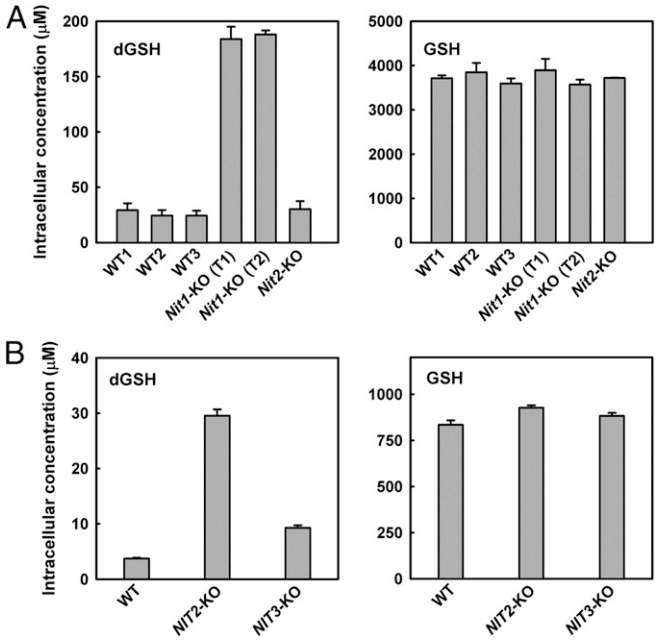

Fig. 2. Accumulation of dGSH in *Nit1*-deficient HAP1 cells and in *NIT2*-deficient yeast. (*A*) HAP1 cell extracts were prepared from two cell lines deficient in *Nit1*, from one HAP1 cell line deficient in *Nit2* and from three control cell lines. Among these, two were cell lines that had been submitted to the CrispR/Cas9 gene inactivation procedure, but yielding no modification of the *Nit1* gene; this was done to exclude the possibility of any off-target effect of the guide RNAs used that may lead to dGSH accumulation. (*B*) WT *S. cerevisiae* and mutants lacking either scNit1 (*NIT2*-KO) (Table 1) or scNit2 (*NIT3*-KO) were cultivated in minimal defined medium with 1% glucose. Samples were collected after 15 h from starting the culture, corresponding to the late exponential growth phase. Intracellular metabolites were extracted, analyzed by LC/MS and dGSH and GSH were quantitated as above. Intracellular concentrations were calculated as detailed in *Materials and Methods*. Means ± SEM of three biological replicates are shown. A modest but statistically significant ($P < 0.05$) increase in the intracellular dGSH concentration was reproducibly observed in *NIT3*-KO cells compared with WT. The *NIT3*-KO cells appeared to accumulate substantial amounts of α-KGM (≥300 μM), and it is possible that the observed increase in dGSH is secondary to this accumulation.

accumulated to about 180 μM (i.e., at least sixfold higher than in the controls). On the other hand, GSH levels did not vary significantly between control cells and Nit1- or Nit2-deficient cells, with estimated intracellular concentrations of ∼3.5 mM in all cases (Fig. 2*A*).

We similarly found that a yeast strain deficient in the Nit1 ortholog (encoded by the *NIT2* gene) (Table 1) accumulated higher levels of dGSH than either the WT strain or the strain deleted in the Nit2 ortholog (encoded by the *NIT3* gene) (*SI Appendix*, Fig. S4*B*). For yeast, unlike for HAP1 cells, estimates of the intracellular levels of metabolites were based on direct cell volume measurements by a Multisizer 3 Coulter Counter (Beckman Coulter). The calculated intracellular concentration of dGSH reached 28 μM, whereas it was three- to sevenfold lower in the controls (Fig. 2*B*). The estimated intracellular concentration of GSH was around 0.9 mM for yeast, and did not change significantly between the KO mutant and the controls.

We also tested urine from a mouse *Nit1*-KO model (23). By LC/MS we were able to demonstrate the presence of dGSH in urine samples from these mice (Fig. 3); the concentration of dGSH assessed by this technique was 1,260 ± 130 μmol·mmol creatinine^{-1} (mean ± SEM, $n = 4$): that is, at least 15-fold higher than that observed in the controls. In fact, the concentration of dGSH in the urine of *Nit1*-KO mice was sufficiently high that it could also be detected by a spectrophotometric assay, in which the α-KG formation was measured through the coupled reactions of Nit1 and GDH, in a cuvette containing a few microliters of urine diluted in reaction buffer. The spectrophotometric assay yielded concentrations of dGSH within twofold of those estimated by LC/MS (687 ± 120 μmol·mmol creatinine^{-1}).

Gas chromatography-mass spectrometry (GC/MS) analysis of urine revealed the presence of a major peak occurring in the urine samples of all tested *Nit1*-KO mice, but almost absent from the urine of all control mice (Fig. 4 *A* and *B*). The MS spectrum of this unknown compound presented the most intense ion (presumably the molecular ion) at *m*/*z* 398. When we subjected purified dGSH to the same GC/MS analysis, we observed the appearance of a peak with the same elution time and MS spectrum (Fig. 4*C*). Analysis of the spectra indicated that this compound corresponds to a trimethylsilyl (TMS) derivative of a dehydrated, dethiolated form of dGSH, presumably generated during derivatization (Fig. 4*D* and *SI Appendix*, Fig. S5). The same *m*/*z* 398 compound was also observed in the GC/MS analysis of extracts from *Nit1*-deficient HAP1 cell lines (*SI Appendix*, Fig. S6).

Formation of dGSH Is a Side Reaction of Numerous Transaminases. The accumulation and excretion of dGSH in model systems suggests that Nit1 is the only (or at least the main) enzyme capable of metabolizing this compound. However, it remains to be established how dGSH is formed in vivo. To address this issue, we investigated the capacity of transaminases to carry out transamination reactions using GSH or OA as amino group donors. We began by focusing on glutamine transaminase K (gene symbol *KYAT1*), a rather promiscuous enzyme known to catalyze transamination reactions with glutamine, as well as with a number of other amino acids (24). Evidence that recombinant KYAT1 is also able to react with GSH is shown in *SI Appendix*, Fig. S7*A*. Addition of GSH led to a progressive change in the enzyme spectrum indicating the conversion of the protein-bound PLP cofactor to pyridoxamine 5′-phosphate. No change took place in the absence of GSH. Similar data were obtained when GSH was replaced with OA.

HPLC analysis of reaction mixtures in which OA and glyoxylate—which has the advantage of binding quite weakly to glutamine transaminase K, limiting the phenomenon of substrate inhibition observed with larger α-keto acid substrates (25, 26)—were incubated overnight with KYAT1 indicated the appearance of two peaks corresponding to dOA (*SI Appendix*, Figs. S7*B* and S8). A similar experiment performed with GSH resulted in the appearance of several peaks, corresponding to a mixture of reduced dGSH and of disulfides resulting from its reaction with GSH or with itself (*SI Appendix*, Figs. S7*C* and S9).

To measure the slow formation of dGSH and dOA by KYAT1 and by other transaminases, we used a coupled assay with Nit1 and GDH. The assay worked well in a continuous format (an example with the enzyme ornithine aminotransferase, OAT, is shown in *SI Appendix*, Fig. S10). However, to minimize artifacts because of contaminating NADH-oxidizing activities or the regeneration of L-Glu by GDH, these coupled assays were performed in a discontinuous fashion. This way we could compare the side-activities leading to dGSH to more classic activities for some representative mammalian transaminases (including both cytosolic and mitochondrial examples) (27) (Table 3). Quite remarkably, detectable activities were encountered in all cases, although they were very small compared with the more classic activities of these enzymes.

To further test whether dGSH in mammalian cells is mostly formed through aminotransferase reactions, we cultured the WT and *Nit1*-deficient HAP1 cell lines in the presence and in the absence of aminooxyacetate (AOA), which is a general inhibitor of

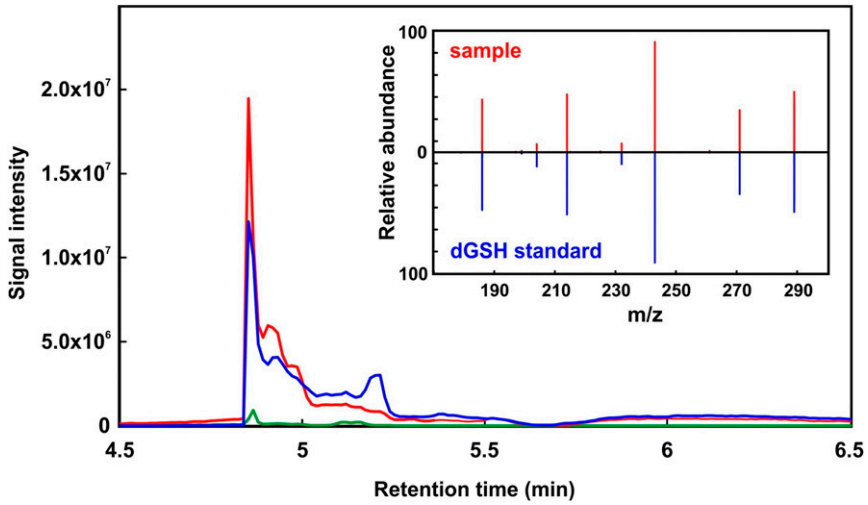

Fig. 3. LC/MS detection of dGSH in the urine of *Nit1*-deficient mice. LC/MS chromatograms showing the presence of dGSH in the urine (500-fold diluted) of a *Nit1*-KO mouse (red line) and a WT mouse (green). The blue chromatogram refers to urine from a WT mouse spiked with 25 μM purified dGSH. (*Inset*) MS2 spectrum of dGSH found in the *Nit1*-KO urine sample, mirrored with the MS2 spectrum generated from the standard.

PLP-dependent enzymes, including transaminases (28). As shown in *SI Appendix*, Fig. S11, the accumulation of dGSH in HAP1 cells decreased in a dose-dependent manner when the cells were cultivated for 24 h with 50, 100, or 200 μM AOA added to the culture medium. These data support the hypothesis that aminotransferase activity is necessary to form dGSH in vivo.

Nit1 Localizes in Both the Cytosol and the Mitochondria of Mammalian Cells. Databases indicate the existence, both in mouse and in humans, of two types of *Nit1* transcripts, which differ by their length at their 5′ end. This suggests that Nit1 can be translated from two distinct, conserved AUGs, resulting in proteins that differ by the presence (mNit1, NP_036179.1) or the absence (cNit1; NP_001229509.1) of a mitochondrial propeptide sequence. Chinese hamster ovary cells were transfected so as to express either form of the Nit1 protein fused at the C terminus to GFP. The transfected cells expressing mNit1-GFP showed localization of the protein mainly in the mitochondria but also in the cytosol, whereas those expressing cNit1-GFP showed exclusively a cytosolic localization (*SI Appendix*, Fig. S12). Overall, this double localization of Nit1 is in agreement with the results of earlier studies (23, 29) and is consistent with a role of the enzyme in recycling a side product of transaminases, which are abundant in both the cytosol and the mitochondria.

Activity of Nit1 and Nit2 Toward α-KG–CoA and Other Potential Substrates. As noted in the introduction, an alternative repair function for Nit1 could be the hydrolysis of α-KG–CoA. An enzyme capable of producing α-KG–CoA is SUGCT [the product of a gene also known as *C7orf10* (30)]. This mitochondrial enzyme reversibly exchanges CoA between a dicarboxylyl-CoA and a dicarboxylate. Its main physiological substrates are succinyl-CoA and glutarate, but in vitro it was shown to use, with lower efficiency, various other dicarboxylates, including α-KG (30).

By using the recombinant human SUGCT, we were able to produce α-KG–CoA and to show that it is hydrolyzed by mmNit1. In fact, among all dicarboxylyl-CoAs that are made by SUGCT, α-KG–CoA was found to be the best mmNit1 substrate, emphasizing that the presence of a keto function on the α-carbon is essential for substrate recognition (*SI Appendix*, Fig. S13*A*). However, mmNit2 also cleaved α-KG–CoA at almost the same rate as that observed with mmNit1 (*SI Appendix*, Fig. S13*B*), indicating that α-KG–CoA hydrolysis is not an activity unique to Nit1, unlike dGSH hydrolysis.

We also further tested the specificity of mmNit1 and of its yeast ortholog with different amides physiologically present in mammalian cells. No activity (< 0.001 μmol/min per milligram protein) was detected by measuring spectrophotometrically the formation of glutamate from L-glutamine, γ-L-glutamyl-ε-L-lysine, *N*-acetyl-aspartylglutamate, or *N*-acetylglutamate (all tested at 1-mM concentration in the presence of 500 nM enzyme). A very low activity was, however, detected with 1 mM GSH as a substrate (Table 4).

Presence of dGSH Amidases and ω-Amidases in Bacteria. BLAST searches indicated that several enteriobacteriaceae, known to contain GSH (as indicated by GSH assays or by the presence in their genomes of both GSH synthetase and γ-glutamylcysteine synthetase), contain two Nit1/Nit2 homologs. The homologs from *Escherichia coli*, *Yersinia enterocolitica*, and *Pseudomonas aeruginosa* were expressed in recombinant form and their activity toward dGSH and α-KGM was tested using a fixed concentration (80 μM) of these substrates. One of the two homologs (YafV in the case of *E. coli*) showed high activity toward α-KGM and almost no detectable activity toward dGSH, whereas the other homolog (YbeM in the case of *E. coli*) showed higher activity with dGSH than with α-KGM. The ratio of the two activities indicates that the *E. coli* enzyme is about as specific as mouse mmNit1 and scNit1, whereas the enzymes of *P. aeruginosa* (paNit1) and *Y. enterocolitica* (yeNit1) are less specific (Table 4).

Similar assays performed on the single Nit1/Nit2 homolog present in the cyanobacterium *Synechocystis*, which like other cyanobacteria contains the GSH synthesizing enzymes, indicated that it acted on both dGSH and α-KGM, with a ratio of activities of only 3.4. In contrast, the single homologs present in *Bifidobacterium longum* and in *Staphylococcus aureus*, which have no GSH synthetase, showed higher activity toward α-KGM, most particularly in the case of the *S. aureus* enzyme, which was ~3,500-fold more active with α-KGM than with dGSH (Table 4).

Remarkably, tests performed to measure glutamate formation from GSH or L-glutamine indicated that, as a rule, the "dGSH amidases" had a low but detectable activity toward GSH and no activity toward L-glutamine, while reciprocally, ω-amidases showed a low activity toward L-glutamine, but no activity toward GSH (Table 4). Thus, the side activities of these enzymes mirrored their main activities toward their physiologic, deaminated substrates.

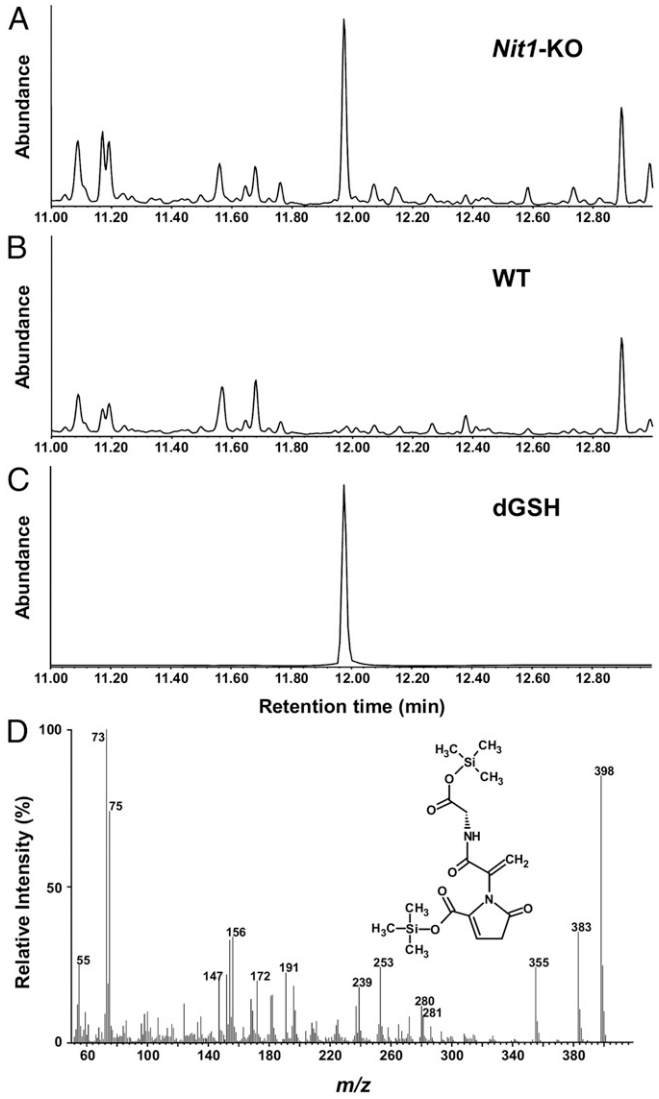

Fig. 4. GC/MS detection of a dGSH derivative in the urine of *Nit1*-deficient mice. Urine samples were treated with the TMS reagent BSFTA/TMCS [*N,O*-bis(trimethylsilyl) trifluoroacetamide-trimethylchlorosilane] (*SI Appendix, Supplementary Materials and Methods*). (*A*) GC/MS total ion current chromatogram showing the presence of a major peak (with retention time 11.97 min and *m/z* 398 for the apparent molecular ion) in the urine of a *Nit1*-KO mouse. The same peak was observed in all of the urine samples from *Nit1*-KO mice. (*B*) In contrast, the peak was undetectable in the urine of control mice. (*C*) GC/MS analysis of purified dGSH shows a peak with the same retention time and mass spectrum (see also *SI Appendix*, Fig. S5), indicating that this is a derivative of dGSH. (*D*) Mass spectrum of the compound present in the urine of *Nit1*-KO mice. The molecular ion shifted to *m/z* 416 upon silylation with *N,O*-Bis (trimethyl-d_9-silyl)acetamide (d_9-BSA) (*SI Appendix*, Fig. S5*C*), indicating that the ion is M^+ and contains two TMS moieties. High-resolution MS indicated the elemental formula $C_{16}H_{26}N_2O_6Si_2$ (exact mass 398.13892; calculated mass 398.13294; millimass error 5.98 and unsaturation of 7.0), implying for the underivatized compound MW = 254 and the elemental formula $C_{10}H_{10}N_2O_6$. The *Inset* shows the proposed structure for the dGSH derivative.

Discussion

Nit1 and Its Yeast Ortholog Hydrolyze dGSH. The role of Nit1 has remained a conundrum, despite intensive studies on this enzyme, including several structural studies (1–6, 23, 31). The results presented here are in agreement with the crystal structure of the yeast Nit1 ortholog, scNit1, which included a GSH-like molecule bound at the active site (31). The crystallized enzyme (catalytically inactivated by the replacement of Cys169 with Ala) had been expressed in *E. coli* (31), which produces GSH. The metabolite repair concept led us to consider the possibility that the substrate of Nit1 may be indeed a modified form of GSH, resulting from minor side activities of transaminases. This hypothesis has been borne out by the overall results of the present study.

The data obtained with purified recombinant enzymes show that, among the potential substrates that we tested, dGSH is by far the best for Nit1. Furthermore, our results with human *Nit1*-KO cells and with *Nit1*-KO mice indicate that dGSH is used by the mammalian Nit1 and its yeast ortholog in vivo. Because it is customary to name enzymes after their best substrate, we propose for Nit1 and its orthologs the name "dGSH amidases." This is not meant to imply that Nit1 does not act on other substrates, but these are most likely quantitatively less important than dGSH (see below). For example, the fact that mmNit1 and mmNit2 display similar activities toward α-KG–CoA, but drastically different activities toward dGSH, suggests that the evolutionary pressure allowing the conservation of Nit1 and its orthologs is based on their capacity to hydrolyze dGSH.

Structural Features Differentiating dGSH Amidases from ω-Amidases. Given their high sequence similarity, it is worthwhile to analyze the features that contribute to the substrate specificities of dGSH amidases and ω-amidases. We show in *SI Appendix*, Fig. S14*A* an alignment of all 13 amidases that have been investigated and a phylogenetic tree that was constructed from this alignment. Remarkably, the enzymes that act preferentially on dGSH and those that act preferentially on α-KGM do not generate two distinct branches (*SI Appendix*, Fig. S14*B*): the *B. longum* enzyme blYbeM acts best on α-KGM, whereas its most similar homolog, *E. coli* YbeM, hydrolyzes dGSH 500-fold better than it does with α-KGM. We noted also from pairwise sequence alignments that mouse ω-amidase (mmNit2) shows a higher degree of identity with mouse or yeast dGSH amidases (35% and 31% identity with mmNit1 and scNit1) than with its *E. coli* ortholog (26% identity with ecYafV). This finding suggests a complex evolutionary history of the Nit1/Nit2 family, where specialization toward enzymes acting as ω-amidases or dGSH amidases may have occurred more than once through convergent evolution. Such a pattern is not surprising considering the intricate history of GSH, which appears to have been "invented" on distinct occasions during evolution (32, 33).

Inspection of the alignment shows that, as expected, all 13 sequences share the catalytic triad (highlighted in yellow) typical of enzymes of the Nit1/Nit2 family (Glu45-Lys127-Cys169, according to the scNit1 numbering). Furthermore, they all share residues (highlighted in cyan) that interact with the α-KG (or oxaloacetyl) moiety of the substrates (*SI Appendix*, Fig. S15), most particularly: (*i*) an Arg residue (Arg173) located four positions after the catalytic Cys; the guanidino group of this Arg interacts with the α-carboxylic group of α-KGM or dGSH in scNit1 (31); (*ii*) a Phe or Trp (Phe195 in scNit1) ~ 25 residues downstream of the catalytic Cys; this residue interacts via π–π interaction with the keto group of α-KG in scNit1 (31), thus impeding recognition of substrates (e.g., GSH in Nit1, L-glutamine in Nit2) where the keto group is replaced by a protonated amine.

As stated in the introduction, a major discriminant between Nit1 and Nit2 is the size of the subpocket where the amido group of α-KGM is predicted to bind. This subpocket is much smaller in mmNit2 (*SI Appendix*, Fig. S15) because of the presence of Tyr87 and Tyr254 (magenta in *SI Appendix*, Fig. S15) (31). The first of these two residues is highly conserved in highly specific ω-amidases; the second residue is also conserved, if one allows for a shift of two positions in the "YafV"-type of ω-amidases (*SI Appendix*, Fig. S14*A*). We propose that these two residues are a signature for ω-amidases.

Table 3. Slow GSH transaminations carried out by five different mammalian transaminases

Enzyme	Amino group donor → Amino group acceptor (3 mM) ↓	Activity (turnovers·min^{-1}) GSH (15 mM)	L-Gln (1 mM)	L-Glu (1 mM)	L-Orn (1 mM)
KYAT1	Glyoxylate	0.17 ± 0.05	42 ± 4	<0.1	—
	4-Methylthio-2-oxobutyrate	0.049 ± 0.003	130 ± 7	<0.1	—
PSAT1	Glyoxylate	0.53 ± 0.14	1.2 ± 0.4	10 ± 2	—
	Oxaloacetate	0.17 ± 0.01	5.7 ± 0.8	23 ± 1	—
GOT1	Glyoxylate	0.018 ± 0.003	0.23 ± 0.02	0.40 ± 0.02	—
	Oxaloacetate	0.012 ± 0.002	7.8 ± 0.7	686 ± 72	—
KYAT3	Glyoxylate	0.04 ± 0.02	51 ± 3	≤0.1	—
	4-Methylthio-2-oxobutyrate	0.012 ± 0.003	25 ± 2	≤0.1	—
OAT	Glyoxylate	0.27 ± 0.06	≤0.1	5.0 ± 0.5	3.3 ± 0.2
	α-KG	—	—	—	187 ± 4

Activities are expressed as number of turnovers per active site per minute, and are the average (± SEM) of at least three separate measurements. The five recombinant transaminases examined in this table are: human glutamine transaminase K [KYAT1; the cytosolic form was tested (27)]; human phosphoserine aminotransferase (PSAT1; cytosolic); human cytosolic aspartate aminotransferase (GOT1); mouse glutamine transaminase L (KYAT3; the cytosolic form was tested); mouse ornithine aminotransferase (OAT; mitochondrial). Enzymatic assays are described in *Materials and Methods*.

Remarkably, in all dGSH amidases, the first of these two residues is replaced by a smaller residue (Ser51 in scNit1; green *SI Appendix*, Fig. S14*A*), which allows for a larger subpocket. The second residue is replaced by a basic residue (Arg250 in scNit1; green in *SI Appendix*, Fig. S14*A*), which interacts with the carboxylic group of the glycine moiety of dGSH (31). Strikingly, this basic residue is conserved in all dGSH amidases, if one allows for a one-residue shift in *E. coli* YbeM (*SI Appendix*, Fig. S14*A*); on the other hand His93, also proposed to interact with the cysteinylglycine moiety of dGSH (31) is not conserved. We therefore propose that a small residue (Gly, Ala, Ser, or Asp) in the first of the two positions and a basic residue in the second position are a signature for dGSH amidases. It is interesting to note that the first, small residue is replaced by a large, polar residue (Arg) in the *B. longum* enzyme (*SI Appendix*, Fig. S14*A*) and that this enzyme is a good ω-amidase and a poor dGSH amidase, unlike ecYbeM with which it clusters in the evolutionary tree. This finding agrees with the importance of this residue for substrate discrimination.

In *SI Appendix*, Table S3, we provide a list of ∼130 organisms with indications about their potential ability to produce GSH (as deduced from the presence of a GSH synthetase and a γ-glutamylcysteine synthetase) and the presence of dGSH amidase or ω-amidase (as deduced from similarity with the enzymes studied in the present work, combined with the presence of the signature residues described above). As summarized in Table 5, most of the organisms that we investigated have both the capacity to synthesize GSH and a putative dGSH amidase or have neither of these. Exceptions are a couple of bacteria whose genomes encode a putative dGSH amidase but no GSH synthetase, which might be because of the existence of an additional form of GSH synthetase that has not yet been identified, as was indeed proposed for *Rubrobacter xylanophilus* and *Rubrobacter radiotolerans* (34). Another exception is a significant group of species that have the capacity to synthesize GSH while not having any dGSH amidase. This finding suggests that this enzyme may be dispensed with or that a nonhomologous enzyme catalyzes the hydrolysis of dGSH in some organisms. Overall, these data indicate

Table 4. Specificity of the amidase activities of Nit1/Nit2 homologs from different bacterial species compared with the mouse and *S. cerevisiae* enzymes

Protein	dGSH amidase specific activity (μmol·min^{-1}·mg^{-1})	ω-Amidase specific activity (μmol·min^{-1}·mg^{-1})	Amidase activities: dGSH /α-KGM	Protein in assay (nM)	GSH amidase specific activity (μmol·min^{-1}·mg^{-1})	L-Glutaminase specific activity (μmol·min^{-1}·mg^{-1})
mmNit1	0.804 ± 0.042	0.002 ± 0.000	530 ± 50	10/600	0.005; 0.008	<0.001
mmNit2	<0.001	7.59 ± 0.29	<0.001	500/2	<0.001	0.003; 0.002
scNit1	8.71 ± 0.13	0.004 ± 0.000	2400 ± 35	2/600	0.003; 0.002	<0.001
scNit2	<0.001	3.59 ± 0.08	<0.001	500/2	<0.001	0.044; 0.037
ecYbeM	40.63 ± 0.27	0.178 ± 0.000	503 ± 3	2/100	0.001; 0.001	<0.001
ecYafV	0.001 ± 0.000	6.65 ± 0.08	<0.001	500/2	<0.001	0.167; 0.172
yeNit1	6.50 ± 0.17	0.20 ± 0.00	33 ± 1	10/100	0.002; 0.003	<0.001
yeYafV*	<0.001	21 ± 0.60*	<0.001	500/2	<0.001	0.002; 0.001
paNit1	13.6 ± 0.75	1.10 ± 0.10	13 ± 0.2	10/10	0.003; 0.004	<0.001
paYafV	<0.001	9.55 ± 0.08	<0.001	500/2	<0.001	0.264; 0.269
syNit1	7.77 ± 0.12	2.13 ± 0.09	3.7 ± 0.1	10/10	<0.001	<0.001
blYbeM	0.11 ± 0.00	2.44 ± 0.03	0.05 ± 0.00	100/10	<0.001	0.001; 0.000
saYafV	0.001 ± 0.000	3.87 ± 0.00	<0.001	4500/2	<0.001	0.011; 0.010

All activities were determined spectrophotometrically at 37 °C. dGSH and ω-amidase was assayed by measuring the formation of α-KG from 80 μM dGSH (column 2) or α-KGM (column 3) as described in *Materials and Methods*. The concentration of enzyme used in these assays is indicated (column 5) for dGSH amidase (first value) and ω-amidase (second value). GSH amidase and L-glutaminase activities were determined spectrophotometrically by the production of L-glutamate from 1 mM GSH or L-glutamine.

*Because of its instability at pH 8.5, all assays with this protein were performed at pH 7.2 (50 mM potassium phosphate).

Table 5. Occurrence of dGSH amidase and GSH synthetase in 133 representative organisms

GSH synthetase	dGSH amidase	No. of instances	Examples
+	+	38	*Danio rerio*, *Drosophila melanogaster*, *Arabidopsis thaliana*, and many proteobacteria and cyanobacteria
—	+	2	*Anaeromyxobacter dehalogenans*, *Salinispora arenicola*
+	—	19	*Trypanosoma brucei*, *Buchnera aphidicola*, *Xylella fastidiosa*
—	—	62	*Encephalitozoon intestinalis*, *Haemophilus influenzae*, *Haemophilus pylori*
+	Dubious	2	*Bradyrhizobium japonicum*
—	Dubious	11	*Arthrobacter alpinus*

Summary of the data presented in *SI Appendix*, Table S3, which comprises eukaryotes, eubacteria, and archaea.

that dGSH amidases are largely distributed in GSH-containing organisms, and extremely rare in others (Table 5).

Nit1 Is Useful to Correct the Unspecific Activity of Transaminases Toward GSH. GSH is one of the most abundant intracellular carriers of an α-amino group. Amino acids are usually present at much lower concentrations, except for glutamate and glutamine. It is therefore not surprising that GSH may be the subject of significant side-reactions.

Transaminases are also abundant cellular enzymes, localized mostly in the cytosol and in the mitochondria. We have tested several transaminases (both cytosolic and mitochondrial) and found that all of them possess some ability to produce dGSH. In other words, the incidental production of dGSH seems to be a feature shared by many transaminases and at least one decarboxylase (35). We use the term incidental, because the observed reaction efficiencies are remarkably small (Table 3). However, even reaction rates of such a modest order of magnitude can become very significant over time, especially when there is ample availability of substrate, as is the case for intracellular GSH.

Besides these considerations, several pieces of circumstantial evidence from model cells and animal systems support a scenario in which the formation of dGSH arises from the "mistaken" reactions of transaminases and that Nit1, by degrading dGSH, fulfills the role of a metabolite repair enzyme.

First, the observation that AOA, a general inhibitor of transaminases, limits the accumulation of dGSH is consistent with the idea that transamination is the major route for dGSH formation in vivo. In principle, dGSH could also be formed through oxidative deamination of GSH, in particular by IL4I1, the mammalian enzyme equivalent to snake venom L-amino acid oxidase. However, expression of this enzyme is exquisitely specific for cells of the immune system and is under the control of IL-4 (36), making it unlikely that IL4I1 can be a main producer of dGSH.

Second, Nit1 is found in the "right" places. We have shown that the mammalian Nit1 is located in both the cytosol and the mitochondria, the two subcellular environments where dGSH-forming transaminases are mainly localized. Additionally, expression of *Nit1* is particularly high in the liver and kidney (23), where transaminase expression is also most abundant.

Third, there is no known metabolic use for dGSH, which in fact is excreted in substantial amounts by *Nit1*-KO mice. In contrast, the products of the Nit1 reaction (α-KG and cysteinylglycine) are readily metabolized (37). These observations are consistent with dGSH representing a "waste" compound, which may require a repair enzyme to be recycled into metabolites useful for the cell.

In principle, transaminations where GSH is the amino group donor could afford the same advantage as transaminations with glutamine. In fact, both processes are essentially irreversible, because the products that are formed cyclize and because they are hydrolyzed by an amidase: Nit2 (in the case of α-KGM) or Nit1 (in the case of dGSH). The metabolic disadvantage of the pathway involving GSH is that resynthesizing GSH from dGSH would cost two ATP molecules compared with one for regenerating glutamine through the glutamine synthase reaction. Furthermore, if transamination reactions with GSH were highly active, the intracellular levels of cysteinylglycine and of its hydrolysis product cysteine might rise substantially. Because cysteine is more reactive and more toxic than is GSH (38), this would represent a liability for the cell.

There has obviously been a counter-selection during evolution to avoid GSH being used as a standard substrate for transamination. Nevertheless, the very presence of Nit1, which can "correct" the formation of dGSH, may conceivably limit the evolutionary pressure for transaminases to achieve an even greater discrimination against GSH, potentially explaining why so many enzymes retain some marginal ability to form dGSH.

It is likely that transaminases catalyze side reactions toward other γ-glutamyl-amino acids or γ-glutamyl-amines that are formed by transglutamylation reactions using GSH as a donor (39). It would be interesting to determine whether the variety of α-KG derivatives that might be formed in this way is processed by Nit1 and its functional orthologs. However, given the abundance of GSH, it is likely that these other potential derivatives are only of minor importance.

Considerations Concerning the Biological Importance of Nit1. The present work establishes a clear link between Nit1 enzyme activity and the metabolism of GSH. The distribution of Nit1 orthologs in disparate (but GSH-producing) organisms attests to the biological importance of the dGSH amidase function and strongly implies that this function provides significant selective advantages. On the other hand, both Nit1-deficient cells and mice do not show any dramatic phenotype, raising the question as to what these advantages can be.

GSH has many recognized functions (40): these include roles as an antioxidant (and as a cofactor for the neutralization of peroxides and related products generated by reactive oxygen species), in the detoxification of xenobiotics, in metal homeostasis, and as a preferred form of cysteine storage and transport. In effect, GSH can be regarded as a "protected," more stable form of cysteine (e.g., less prone to autooxidation) (41).

An obvious advantage of having a dGSH amidase is therefore to avoid the loss of GSH (and hence of L-cysteine); this can be best appreciated by considering the case of the mammalian enzyme. If the levels of dGSH excretion observed in mice (we consider here the lowest estimate, 687 μmol·mmol creatinine^{-1}) were applicable to humans, a 70-kg individual deficient in *Nit1* would excrete daily about 2.2 g of GSH as dGSH. Such an amount corresponds to ∼15% of total body GSH. By comparison, individuals with γ-glutamyl transpeptidase deficiency were reported to eliminate in urine up to 1 g GSH per day (42).

Given the high rate at which GSH is turned over, this drain of GSH may be overcome and cause no harm under most conditions. Indeed, the accumulation of dGSH in *Nit1*-KO cell models does not appear to significantly affect the GSH levels in the same cells (Fig. 2). However, it seems reasonable to hypothesize that the depletion of GSH may be less sustainable in cells particularly rich in transaminases or in times when the GSH demand is high. In addition to this hypothesis, the accumulation of dGSH might also subtly alter some cellular functions. For example, because there are many enzymes (including oxidoreductases and glutathione

S-transferases) that use GSH as a substrate, dGSH may potentially interfere with the function of at least some of them. In the long term, these phenomena may represent a sizable selective disadvantage for the Nit1-deficient organisms.

Nit1 was classified as a tumor suppressor because of its association with the fragile histidine-triad protein Fhit. In fact, whereas Nit1 and Fhit are discrete proteins in mammals, they are expressed as fused domains in widely distant invertebrates such as nematodes, insects, arthropods, and flatworms (2, 23). Fhit proteins act best to hydrolyze adenyl-derivatives, such as ApppA and AppppA (1, 2). However, we do not see any obvious connection between the enzymic functions of Fhit and of Nit1. We must also stress that, although data collected in mammalian cells, mice models, and human samples suggest that Nit1 promotes apoptosis (23) and affects, in a complex fashion, the development and progression of some types of tumors (23, 43), it is uncertain whether these roles bear any connection with the enzyme's catalytic function. In fact, mutation of the conserved active site cysteine to an alanine did not alter the ability of Nit1 to promote apoptosis in human cells (23). Perhaps related to the above, a recent study reported that Nit1 can interact with β-catenin, repressing β-catenin–mediated transcription, and that this repressive activity is not affected by mutation of the catalytic cysteine (44). It is therefore possible that the Fhit–Nit1 connection may reflect other (as yet unclearly defined) Nit1 functions that do not depend on the catalytic hydrolysis of dGSH.

Concluding Remarks

The results presented here establish Nit1 as a new example of a highly conserved enzyme with a metabolite repair role. Further work will be needed to understand why the dGSH amidase activity of Nit1 is important. Is it because dGSH exerts some toxic effects in the cells or is it to recycle precious building blocks? In any case, this work suggests that, when addressing the function of the numerous putative enzymes encoded by the human and other genomes, their possible involvement in metabolite repair should be seriously considered. The enormous chemical diversity that side reactions add to the metabolome makes this search for enzymic function both more challenging and more interesting.

Materials and Methods

Materials and other methods used in this work are mainly provided in the *SI Appendix*. All procedures involving mice were performed following protocols approved by the Ohio State University Institutional Animal Care and Use Committee.

Cloning, Overexpression, and Purification of Recombinant Proteins. His_6-tagged (mouse) mmNit1 (lacking the targeting peptide sequence) and mmNit2 were expressed as reported earlier (5). The human cytosolic transaminases, glutamine transaminase K (KYAT1; previously CCBL1), aspartate aminotransferase (GOT1), and phosphoserine aminotransferase (PSAT1) were expressed as described previously (25). The coding sequences of the yeast Nit1 and Nit2 orthologs (encoded by the *NIT2* and *NIT3* genes, respectively), and of the bacterial homologs shown in Table 1, with the exception of ecYafV and blYbeM, were PCR-amplified from genomic DNA, cloned in the pET28a vector, and expressed as recombinant proteins (N-terminal His6 tag) in *E. coli* BL21(DE) cells. ecYafV was expressed from an ASKA clone (45) and blYbeM was produced using a pET28A plasmid containing a codon optimized synthetic sequence (GenScript). The coding sequences of mouse ornithine transaminase (OAT) and glutamine transaminase L (official gene symbol KYAT3; previously CCBL2) were PCR-amplified from mouse cDNA and cloned into expression vectors (pET28a and pET24, respectively); the proteins were then expressed in recombinant form in *E. coli* BL21(DE) cells. Details of (*i*) the primers used for PCR amplification, (*ii*) the restriction enzymes used for cloning, and (*iii*) the culture conditions adopted for the overexpression of individual proteins are provided in *SI Appendix, Supplementary Materials and Methods*. Preparation of bacterial homogenates and purification of recombinant proteins by metal-affinity chromatography (HisTrap columns) were carried out as previously described (46). Purified proteins were finally kept in 25 mM Hepes, pH 7.2, 300 mM NaCl, 1 mM DTT, and 10% (vol/vol) glycerol, and stored at −70 °C until use.

Production of HAP1 Cell Lines Deficient in Nit1 and Nit2 by CRISPR/Cas9. The human-derived HAP1 cell line (Horizon Discovery) expresses both the *Nit1* and the *Nit2* genes, as described by the number of transcripts per kilobase million for Nit1 (13.85; https://www.horizondiscovery.com/human-nit1-knockout-cell-line-hzghc4817) and for Nit2 (53.21; https://www.horizondiscovery.com/human-nit2-knockout-cell-line-hzghc56954). The parental cells were therefore used to create HAP1 cell lines deficient in either Nit1 or Nit2 by the CRISPR/Cas9 technology (details provided in *SI Appendix, Supplementary Materials and Methods*).

The clones we ultimately selected for further studies presented the following modifications in the *Nit1* or *Nit2* genes: for Nit1-T1, a 13-bp deletion, leading to a change in reading frame after the codon for Val-71 and a premature stop 18 codons later; for Nit1-T2, a >190-bp insertion after the codon for Asn179, which also leads to a premature stop after about 40 codons; finally, for NIT2, an 80-bp insertion after Glu64, with a premature stop after 20 codons.

Preparation of Amidase Substrates. α-KGM was prepared by oxidation of L-glutamine by snake venom L-amino acid oxidase, as previously described (5). dGSH and dOA were prepared by an analogous procedure. Briefly, a 200-mM solution of GSH or OA, adjusted to pH 7, was incubated overnight at 37 °C under agitation with 4 units/mL of catalase and 2 mg/mL of *Crotalus adamanteus* L-amino acid oxidase (Sigma). After incubation, the reaction mixture for the preparation of dGSH was usually supplemented with solid DTT (~120 mM final) to reduce the disulfide adducts. The mixture was then deproteinized by addition of $HClO_4$ to a final concentration of 3% and centrifuged at 15,000 × *g* for 15 min at 4 °C. A first purification of the products from reagents was accomplished by applying the supernatant to a 5 mL AG50 cation-exchange column, equilibrated with 0.1 M HCl. The eluate was neutralized with 3 M K_2CO_3, and the $KClO_4$ precipitate was removed by centrifugation. dGSH and dOA were further purified by HPLC from a 19 × 150 mm XBridge Prep C18 column (Waters), by isocratic elution with 3% aqueous acetonitrile/0.1% trifluoroacetic acid at a flow rate of 20 mL/min. Both reduced dGSH (*m/z* 307, detected as $[MH]^+$) and dOA (*m/z* 289) eluted in two adjacent peaks of similar areas, attributable to the two anomeric forms of the cyclized ketoacids. This finding was supported by the observation that the compounds in both peaks were substrates for Nit1.

ω-Amidase Assay. The reaction of mmNit2 and its orthologs was monitored through a coupled assay with GDH (5). Measurement of this reaction is complicated by the fact that α-KGM essentially exists in cyclic forms, which at equilibrium are about 300 times more abundant than the linear form. The rate of equilibration between the cyclic and linear structure is pH-dependent, being faster at alkaline pH. As only the open form appears to be a substrate for mmNit2 (5, 20), the ω-amidase reaction was measured at pH 8.5 and using very diluted enzyme (1–2 nM). The reaction mixture (1-mL final volume) contained 50 mM Bicine (pH 8.5), 50 mM KCl, 0.5 mg/mL BSA, 2 mM DTT, 0.22 mM NADH, 5 mM ammonium acetate, 2.4 units/mL GDH, as well as the amidase. These assays were performed at 30 °C (results shown in Table 2) or 37 °C (results shown in Table 4). Under these conditions, the measured activity increased linearly with ω-amidase concentration, indicating that the reaction was not rate-limited by opening of the cyclic form of α-KGM. The range of α-KGM concentrations tested was 40–1,500 μM.

dGSH Amidase Assay. Release of α-KG from dGSH and dOA by Nit1 and its orthologs was measured through a coupled assay with GDH, analogous to the ω-amidase assay. The reaction mixture (1 mL) contained 50 mM buffer (Bicine or Hepes), 50 mM KCl, 0.5 mg/mL BSA, 2 mM DTT, 0.22 mM NADH, 5 mM ammonium acetate and 2.4 units/mL GDH. These assays were performed at 30 °C (results shown in Table 2) or 37 °C (results shown in Table 4). When these reactions were performed to determine the enzyme catalytic parameters with dGSH, the buffer used was Bicine pH 8.5 and the concentration of the amidase enzyme was maintained in the range 10–40 nM (mmNit1) or 10–20 nM (scNit1). Under these conditions, the measured activity depended linearly on amidase concentration, indicating that the process was not rate-limited by opening of the cyclic form of the substrate. The range of dGSH concentrations tested was 15–330 μM.

GSH and Other Transamination Assays. Transaminases (1–5 μM) were incubated for up to 24 h at 30 °C, in the presence of GSH (5 or 15 mM) and of an appropriate amino group acceptor in 50 mM Bicine buffer pH 8.5, 50 mM KCl, 0.5 mg/mL BSA, 2 mM DTT. The final volume of the reaction mixture was

typically 0.6 mL. At given times, aliquots (120 μL) were taken from the reaction mixture and heated at 100 °C for 5 min to stop the reaction. The protein precipitate was removed by centrifugation and the content of dGSH in the aliquot was assessed spectrophotometrically through the coupled Nit1-GDH assay described above. Other transaminase assays shown in Table 3 are described in *SI Appendix, Supplementary Materials and Methods*.

Other Specificity Assays. The GSH amidase and the L-glutaminase activities of all amidases (shown in Table 4) were tested in the presence of 1 mM substrate by measuring spectrophotometrically at 37 °C the formation of glutamate. The reaction mixture (1-mL final volume) contained 50 mM Bicine (pH 8.5), 50 mM KCl, 0.5 mg/mL BSA, 2 mM DTT, 0.2 mM NAD^+, 0.5 mM ADP-Mg, 3.5 units/mL GDH, as well as the amidase (100–500 nM). The amidase activity (glutamate producing) of mmNit1 and scNit1 (500 nM in the assay) toward 1 mM γ-L-glutamyl-ε-L-lysine, *N*-acetyl-aspartylglutamate or *N*-acetylglutamate was tested using the same assay.

LC/MS Analyses. Full scans (307–312 *m/z*) for monoisotopic mass detection and natural isotope distribution, selected ion monitoring (307.06 *m/z* and 308.09 *m/z* for dGSH and GSH, respectively, using a measurement window of 0.5 *m/z*) for absolute and relative quantification, and parallel reaction monitoring (307.06 *m/z* and 308.09 *m/z* parent ions, respectively, detecting 50–300 *m/z* fragments) were performed on all samples in separate runs. Standards were prepared in a matrix as close to the samples as possible. For the analysis of yeast and mammalian cell extracts, standard curves of GSH and dGSH were prepared in LC/MS grade water:MeOH (50:50). For the analysis of mouse urine, dGSH standard curves were prepared in urine from a WT mouse. Details on the instrument used, type of column, and separation protocols for GSH and dGSH determination are provided in *SI Appendix, Supplementary Materials and Methods*.

ACKNOWLEDGMENTS. We thank Drs. Yoshito Inoue and Morimasa Ohse (Kanazawa Medical University) and Mrs. Nathalie Chevalier (de Duve Institute, Université Catholique de Louvain) for excellent technical assistance, and Dr. Juliette Létoquart (de Duve Institute) for her help in the preparation of *SI Appendix*, Fig. S15. The E.V.S. laboratory is supported by a WELBIO grant of the Walloon Region, by the Fonds de la Recherche Scientifique Médicale, by the Belgian National Lottery, and by the Interuniversity Attraction Poles Programme initiated by the Belgian Science Policy Office (Grant P7/43 to E.V.S.). M.V.d.-C. and G.T.B. are "Chercheurs qualifié" of the Fonds National de la Recherche Scientifique. The C.L.L. laboratory is supported by the Fonds National de la Recherche Luxembourg Grants CORE C13/BM/5773107 and AFR-PDR (Aides à la Formation-Recherche postdoctoral research) 9180195 (to K.W.E.).

1. Pekarsky Y, et al. (1998) Nitrilase and Fhit homologs are encoded as fusion proteins in *Drosophila melanogaster* and *Caenorhabditis elegans*. *Proc Natl Acad Sci USA* 95: 8744–8749.
2. Pace HC, et al. (2000) Crystal structure of the worm NitFhit Rosetta Stone protein reveals a Nit tetramer binding two Fhit dimers. *Curr Biol* 10:907–917.
3. Barglow KT, Cravatt BF (2006) Substrate mimicry in an activity-based probe that targets the nitrilase family of enzymes. *Angew Chem Int Ed Engl* 45:7408–7411.
4. Barglow KT, et al. (2008) Functional proteomic and structural insights into molecular recognition in the nitrilase family enzymes. *Biochemistry* 47:13514–13523.
5. Jaisson S, Veiga-da-Cunha M, Van Schaftingen E (2009) Molecular identification of omega-amidase, the enzyme that is functionally coupled with glutamine transaminases, as the putative tumor suppressor Nit2. *Biochimie* 91:1066–1071.
6. Krasnikov BF, et al. (2009) Identification of the putative tumor suppressor Nit2 as omega-amidase, an enzyme metabolically linked to glutamine and asparagine transamination. *Biochimie* 91:1072–1080.
7. Meister A, Levintow L, Greenfield RE, Abendschein PA (1955) Hydrolysis and transfer reactions catalyzed by omega-amidase preparations. *J Biol Chem* 215:441–460.
8. Cooper AJ, Meister A (1977) The glutamine transaminase-omega-amidase pathway. *CRC Crit Rev Biochem* 4:281–303.
9. Cooper AJ, et al. (2016) ω-Amidase: An underappreciated, but important enzyme in L-glutamine and L-asparagine metabolism; relevance to sulfur and nitrogen metabolism, tumor biology and hyperammonemic diseases. *Amino Acids* 48:1–20; erratum in 2015, *Amino Acids* 47:2671–2672.
10. Galperin MY, Koonin EV (2004) 'Conserved hypothetical' proteins: Prioritization of targets for experimental study. *Nucleic Acids Res* 32:5452–5463.
11. Galperin MY, Koonin EV (2010) From complete genome sequence to "complete" understanding? *Trends Biotechnol* 28:398–406.
12. Linster CL, Van Schaftingen E, Hanson AD (2013) Metabolite damage and its repair or pre-emption. *Nat Chem Biol* 9:72–80.
13. Van Schaftingen E, et al. (2013) Metabolite proofreading, a neglected aspect of intermediary metabolism. *J Inherit Metab Dis* 36:427–434.
14. Rzem R, et al. (2004) A gene encoding a putative FAD-dependent L-2-hydroxyglutarate dehydrogenase is mutated in L-2-hydroxyglutaric aciduria. *Proc Natl Acad Sci USA* 101: 16849–16854.
15. Van Schaftingen E, Rzem R, Veiga-da-Cunha M (2009) L-2-Hydroxyglutaric aciduria, a disorder of metabolite repair. *J Inherit Metab Dis* 32:135–142.
16. Collard F, et al. (2016) A conserved phosphatase destroys toxic glycolytic side products in mammals and yeast. *Nat Chem Biol* 12:601–607.
17. Gerlt JA, et al. (2011) The enzyme function initiative. *Biochemistry* 50:9950–9962.
18. Meister A (1953) Preparation and enzymatic reactions of the keto analogues of asparagine and glutamine. *J Biol Chem* 200:571–589.
19. Meister A, Otani TT (1957) Omega-amide and omega-amino acid derivatives of alpha-ketoglutaric and oxalacetic acids. *J Biol Chem* 224:137–148.
20. Hersh LB (1971) Rat liver omega-amidase. Purification and properties. *Biochemistry* 10:2884–2891.
21. Buell MV, Hansen RE (1960) Reaction of pyridoxal-5-phosphate with aminothiols. *J Am Chem Soc* 82:6042–6049.
22. Bar-Even A, et al. (2011) The moderately efficient enzyme: Evolutionary and physicochemical trends shaping enzyme parameters. *Biochemistry* 50:4402–4410.
23. Semba S, et al. (2006) Biological functions of mammalian Nit1, the counterpart of the invertebrate NitFhit Rosetta stone protein, a possible tumor suppressor. *J Biol Chem* 281:28244–28253.
24. Cooper AJ, et al. (2008) Substrate specificity of human glutamine transaminase K as an aminotransferase and as a cysteine S-conjugate β-lyase. *Arch Biochem Biophys* 474: 72–81.
25. Donini S, et al. (2009) Recombinant production of eight human cytosolic aminotransferases and assessment of their potential involvement in glyoxylate metabolism. *Biochem J* 422:265–272.
26. Schiroli D, Peracchi A (2015) A subfamily of PLP-dependent enzymes specialized in handling terminal amines. *Biochim Biophys Acta* 1854:1200–1211.
27. Malherbe P, Alberati-Giani D, Kohler C, Cesura AM (1995) Identification of a mitochondrial form of kynurenine aminotransferase/glutamine transaminase K from rat brain. *FEBS Lett* 367:141–144.
28. Korangath P, et al. (2015) Targeting glutamine metabolism in breast cancer with aminooxyacetate. *Clin Cancer Res* 21:3263–3273.
29. Sun J, et al. (2009) Nit1 and Fhit tumor suppressor activities are additive. *J Cell Biochem* 107:1097–1106.
30. Marlaire S, Van Schaftingen E, Veiga-da-Cunha M (2014) C7orf10 encodes succinate-hydroxymethylglutarate CoA-transferase, the enzyme that converts glutarate to glutaryl-CoA. *J Inherit Metab Dis* 37:13–19.
31. Liu H, et al. (2013) Structures of enzyme-intermediate complexes of yeast Nit2: Insights into its catalytic mechanism and different substrate specificity compared with mammalian Nit2. *Acta Crystallogr D Biol Crystallogr* 69:1470–1481.
32. Copley SD, Dhillon JK (2002) Lateral gene transfer and parallel evolution in the history of glutathione biosynthesis genes. *Genome Biol* 3:research0025.
33. Fahey RC (2013) Glutathione analogs in prokaryotes. *Biochim Biophys Acta* 1830: 3182–3198.
34. Johnson T, Newton GL, Fahey RC, Rawat M (2009) Unusual production of glutathione in Actinobacteria. *Arch Microbiol* 191:89–93.
35. Novogrodsky A, Meister A (1964) Control of aspartate beta-decarboxylase activity by transamination. *J Biol Chem* 239:879–888.
36. Mason JM, et al. (2004) IL-4-induced gene-1 is a leukocyte L-amino acid oxidase with an unusual acidic pH preference and lysosomal localization. *J Immunol* 173: 4561–4567.
37. Josch C, Klotz LO, Sies H (2003) Identification of cytosolic leucyl aminopeptidase (EC 3.4.11.1) as the major cysteinylglycine-hydrolysing activity in rat liver. *Biol Chem* 384: 213–218.
38. Cooper AJ (1997) Glutathione in the brain: Disorders of glutathione metabolism. *The Molecular and Genetic Basis of Neurological Disease*, eds Rosenberg R, Prusiner S, DiMauro S, Barchi R (Butterworth-Heinemann, Boston), 2nd Ed, pp 1195–1230.
39. Keillor JW, Castonguay R, Lherbet C (2005) Gamma-glutamyl transpeptidase substrate specificity and catalytic mechanism. *Methods Enzymol* 401:449–467.
40. Aoyama K, Watabe M, Nakaki T (2008) Regulation of neuronal glutathione synthesis. *J Pharmacol Sci* 108:227–238.
41. delCardayre SB, Stock KP, Newton GL, Fahey RC, Davies JE (1998) Coenzyme A disulfide reductase, the primary low molecular weight disulfide reductase from *Staphylococcus aureus*. Purification and characterization of the native enzyme. *J Biol Chem* 273:5744–5751.
42. Griffith OW, Meister A (1980) Excretion of cysteine and gamma-glutamylcysteine moieties in human and experimental animal gamma-glutamyl transpeptidase deficiency. *Proc Natl Acad Sci USA* 77:3384–3387.
43. Wang YA, et al. (2016) Nitrilase 1 modulates lung tumor progression in vitro and in vivo. *Oncotarget* 7:21381–21392.
44. Mittag S, et al. (2016) A novel role for the tumour suppressor Nitrilase1 modulating the Wnt/β-catenin signalling pathway. *Cell Discovery* 2:15039.
45. Kitagawa M, et al. (2005) Complete set of ORF clones of *Escherichia coli* ASKA library (a complete set of *E. coli* K-12 ORF archive): Unique resources for biological research. *DNA Res* 12:291–299.
46. Gemayel R, et al. (2007) Many fructosamine 3-kinase homologues in bacteria are ribulosamine/erythrulosamine 3-kinases potentially involved in protein deglycation. *FEBS J* 274:4360–4374.

Nit1 is a metabolite repair enzyme that hydrolyzes deaminated glutathione

Alessio Peracchi, Maria Veiga-da-Cunha, Tomiko Kuhara, Kenneth W. Ellens, Nicole Paczia, Vincent Stroobant, Agnieszka K. Seliga, Simon Marlaire, Stephane Jaisson, Guido T. Bommer, Jin Sun, Kay Huebner, Carole L. Linster, Arthur J. L. Cooper, Emile Van Schaftingen

SI APPENDIX - SUPPLEMENTARY MATERIALS AND METHODS

Materials. GSH was from Sigma. OA was purchased from Bachem. 2-Aminobutyrylglycine was synthesized in-house on a solid phase using standard Fmoc (fluorenylmethoxycarbonyl) chemistry, purified by reverse-phase high-pressure liquid chromatography (HPLC), and characterized by mass spectrometry. HisTrap HP columns were from Qiagen. Phusion polymerase and restriction enzymes were from NEB. pET expression plasmids were from Novagen. Beef liver glutamate dehydrogenase (GDH) was from Roche Applied Science.

Details on the cloning and expression procedures related to the recombinant proteins produced in this study. The coding sequences of scNit1 (product of the yeast gene *NIT2*; see Table 1 in the main text) and scNit2 (product of the yeast gene *NIT3*) were PCR-amplified from *S. cerevisiae S288C* genomic DNA. The coding sequences for the bacterial proteins were amplified from the genomic DNA of the bacterial strains shown in Table S3. The coding sequences of mouse ornithine transaminase (OAT) and glutamine transaminase L (official gene symbol KYAT3; previously CCBL2) were amplified from a mouse liver cDNA library. Details on the amplification and cloning procedure are summarized below:

	PCR Primers	Vector	Restriction sites
scNit1	Fw: AATTGCTAGCATGACTAGTAAATTAAAACGGGTTG Re: TAATGCGGCCGCTCAATGAAATAAATCGTCTCTTCTC	pET28a	NheI, NotI
scNit2	Fw: TATAGCTAGCATGAGTGCTTCGAAGATTCTTTC Re: ATTTGCGGCCGCTCAATGCGCATTTACATCGGAGTAC	pET28a	NheI, NotI
KYAT3	Fw: ATATGCTAGCATGGCTTTGAAATTCAAAAACGC Re: TAATGCGGCCGCGTCAAGACTTCTGGCTGTTCC	pET24	NheI, NotI
OAT	Fw: ATATCATATGACAGAGCAAGGCCCACCATC Re: ATATGCGGCCGCTCAGAAGGACAAGATAGTCTTG	pET28a	NdeI, NotI
ecYbeM	Fw: AATACATATGCTGGTTGCCGCAGGAC Re: ATTTCTCGAGTCATAATAATTGCGGCGGCGC	pET28a	NdeI, XhoI
yeNit1	Fw: TTAATTGCTAGCATGAAAAATGCCAATGTTGCATTAT Re: AATTGCGGCCGCTTATTTAGATGATTGTTTTGAATCAG	pET28a	NheI, NotI
yeYafV	Fw: TTAATTCATATGTCAACTTTAAAACTAACTCTG Re: TTAATTCTCGAGTTACAACAACAAAAACTTATCGCT	pET28a	NdeI, XhoI
paNit1	Fw: TTAATTCATATGTCCATTGCCGTGATCCAG Re: TTAATTCTCGAGTCACTCCGTACGCGCCGG	pET28a	NdeI, XhoI
paYafV	Fw: TTAATTCATATGCGCGATCTGACGGTTCT Re: TTAATTCTCGAGTCAAGGATGGATTTCGAAGCGA	pET28a	NdeI, XhoI
syNit1	Fw: TTAATTCATATGAAACCGTATTTAGCCGCTG Re: TTAATTCTCGAGTCAGACAAATACCCGATGTTGC	pET28a	NdeI, XhoI
saYafV	Fw: TTAATTCATATGAAAGTCCAAATTTATCAATTAC Re: TTAATTCTCGAGTTATTTATACAAATCTAATTTAATAC	pET28a	NdeI, XhoI

Restriction sites on the primers are underlined. Sequences corresponding to the orf start codon (when present) are shaded in green. Sequences corresponding to the stop codon are shaded in red.

After sequence verification of the cloned inserts, the plasmids were used to transform *E. coli* BL21(DE) cells. Cells were used to inoculate 200 ml of medium and grown in 1-L flasks, under vigorous agitation. When the absorption at 600 nm reached approximately 0.6 OD, protein expression was induced with 0.4 mM IPTG. The specific culture conditions adopted, overall yields and features of the recombinant proteins were as follows.

	Growth conditions	Yield (mg/200 ml)	Protein size(aa)	His_6 tag
scNit1	LB medium, 30°C	1.2	330	N-terminal
scNit2	M9 medium, 30°C	20	314	N-terminal
KYAT3	M9 medium, 30°C	0.7	435	C-terminal
OAT	M9 medium, 30°C	3.8	428	N-terminal
ecYbeM	LB medium, 30°C	6.2	282	N-terminal
ecYafv	LB medium, 30°C	12.4	256	N-terminal
yeNit1	LB medium, 30°C	1	286	N-terminal
yeYafV	LB medium, 30°C	7.3	256	N-terminal
paNit1	LB medium, 30°C	6.6	282	N-terminal
paYafV	LB medium, 30°C	34.8	264	N-terminal
syNit1	LB medium, 30°C	9.9	272	N-terminal
blYbeM	LB medium, 30°C	12.4	276	N-terminal
saYafV	LB medium, 30°C	27.5	261	N-terminal

Generation of mutant yeast strains. The *S. cerevisiae* strains used in this study (**Table S1**), all isogenic to the reference FY4 strain, were generated via PCR-mediated gene replacement (*yNit2*-KO and *yNit3*-KO mutants; primers listed in **Table S2**) as described previously (1, 2).

Yeast metabolite extraction and sample preparation for LC-MS analyses. Yeast strains were grown and monitored as described previously (2), with the exception that the strains used in the present study were prototrophic and thus did not require nutritional supplements. To monitor the growth of yeast cultures, biovolume and cell concentration were determined in aliquots taken from the yeast cultivations using a Multisizer Z3 equipped with a 30-µm measurement capillary (Beckman Coulter) after dilution in ISOTON II solution (Beckman Coulter). Yeast extracts were prepared according to the protocol for yeast metabolome analysis described previously (2). The only difference in procedure was the use of a 30-fold volume of extraction fluid (1 ml per 35 µl of biovolume) for extraction of intracellular metabolites.

Collection of urine from wild-type and *Nit1*-KO mice. The *Nit1*-KO mice have been described (3). For urine collection, mice were grasped and immediately held heads up above parafilm, so that urine was secreted onto the film (4). The urine was pipetted into tubes on dry ice and stored at -80˚C. Given the small volume attainable at each collection (300 µl at most) the samples used in this study were generally combined from multiple urine collections from the same mouse. The age of *Nit1*-KO mice (2 males and 2 females) and control mice (4 sex-matched controls) at the time of collection ranged from 3 to 20 months.

Preparation of urine for LC-MS analysis. LC-MS analysis was performed on the urine of four Nit1-KO mice (two males and two females) and of four sex-matched controls, which were shipped in dry ice to the receiving laboratory. These samples were prepared for metabolomics analysis by centrifugation at 16,100 × g for 15 minutes at 4˚C. The supernatant

was transferred to a glass HPLC vial and stored at -20˚C if not analyzed promptly after preparation.

Details on the production and culture of HAP1 cell lines deficient in Nit1 and Nit2 used in this study. The CRISPR/Cas9 constructs generated to inactivate these genes were prepared starting from two different primer pairs for *Nit1*-target 1 : (CRISP-hNIT1-T1-s1 CACCGgtgtctggcgtcgatgttacc, CRISP-hNIT1-T1-as1 AAACggtaacatcgacgccagacacC and CRISP-hNIT1-T1-s2 CACCGgatgtgctgagctggttcgag, CRISP-hNIT1-T1-as2 AAACctcgaaccagctcagcacatcC), for *Nit1*-target 2 (CRISP-hNIT1-T2-s1 CACCGgtcacctgtcagcacaccagc, CRISP-hNIT1-T2-as1 AAACgctggtgtgctgacaggtgacC and CRISP-hNIT1-T2-s2 CACCGgtagagttgctttcacacat, CRISP-hNIT1-T2-as2 AAACatgtgtgaaagcaactctacC) and for *Nit2* (CRISP-hNIT2-s1 CACCGgtgcagcatatatctcattgg, CRISP-hNIT2-as1 AAACccaatgagatatatgctgcacC and CRISP-hNIT2-s2 CACCGgagcttctgtgtggattcacc, CRISP-hNIT2-as2 AAACggtgaatccacacagaagctcC).
Annealed primer pairs were ligated into the vector pSpCas9n(BB)-2A-Puro (PX462) V2.0 (a gift from F. Zhang, Massachusetts Institute of Technology; Addgene plasmid no. 62987) (5) digested by BbsI. Constructs were validated by sequencing (Beckman Coulter Genomics).
HAP1 cells were cultured in IMDM (Iscove's Modified Dulbecco's Medium) containing 10% FBS, 2 mM L-glutamine and penicillin/streptomycin (Life Technologies). Cells were transfected with the CRISP constructs exactly as described in (6). Genomic DNA from puromycin resistant clones was used to PCR-amplify the regions encompassing the targeted sites and the PCR products were sequenced to evaluate the gene modification present in each clone.

Sample preparation of HAP1 cell extracts for LC-MS analysis. HAP1 cells (10^6) were seeded in 6-well plates and incubated in IMDM with 10% FBS for 24 h with a change of medium occurring approximately 6 hours before extraction. Confluency was about 70-80%. For the extraction, the medium was aspirated and the cells were gently washed with 2 ml of ice-cold 0.9% NaCl. The NaCl solution was removed by aspiration and the plate was placed on ice, after which 800 µl of extraction fluid - 50% methanol, 50% (v/v) TE buffer, pH 7.0, containing 50 mM Tris-HCl and 1 mM EDTA, at -20 °C - was added to the well. Cells were scraped and the mixture was transferred to an Eppendorf tube followed by the addition of 400 µl of chloroform. The mixture was incubated at 4°C in an Eppendorf shaker for 40 min and then centrifuged for 10 min at 10,000 × g (4°C). The upper aqueous phase was removed, filtered (0.22 µm cellulose acetate membrane) and stored at -20 °C until LC-MS analysis. The protein precipitate was dried and redissolved in 0.1 M NaOH for protein quantification (Bradford). The total intracellular volume of the culture was estimated assuming a ratio of 2.5 µl cell water per mg of protein.

LC-MS analyses. LC-HESI-HRMS (liquid chromatography-heated electrospray ionization-high resolution mass spectrometry) measurements were performed on a Dionex UltiMate 3000 UHPLC (ultra-high performance liquid chromatography) apparatus (Thermo Fisher Scientific) coupled to a Q Exactive Orbitrap mass spectrometer equipped with a heated electrospray ionization source (Thermo Fisher Scientific). Nitrogen was supplied by a Genius 1022 high purity generator (Peak Scientific Instruments Ltd). For all measurements, a Zic HILIC Sequant column (150 × 4.6 mm, 3.5 µm particle size, 100 Å pore size; Merck KgAA) connected to a guard column (SecurityGuard ULTRA cartridge, UHPLC HILIC for 2.1 mm ID columns, Phenomenex) was used at 15 °C and at a constant flow of 0.4 ml/min in gradient mode using buffers A (water-acetonitrile-formic acid, 99:1:0.1 by volume) and B (acetonitrile-water-formic acid, 99:1:0.1 by volume) for separation. For the detection of GSH

and dGSH, a 20-min chromatographic gradient was applied, according to the following profile: 0 min - 95 % B, 3 min – 95 % B, 3.5 min – 50 % B, 5 min – 50 % B, 7 min – 5 % B, 17 min – 5 % B, 17.1 min – 95 % B, 20 min – 95 % B. Mass spectral data were obtained in positive ionization mode. Sheath gas flow rate was set to 53, spray voltage to 4.5 kV and the capillary temperature to 269 °C.

Extraction of metabolites from HAP1 cells and derivatization for GC-MS analysis. Adherent HAP1 cells in 3-cm wells were washed once with ice-cold NaCl (0.9%). Immediately thereafter, 500 µl dry-ice-cold methanol and then 500 µl cold water were added per well, and the cells were scraped. Extracts were mixed with 1 ml chloroform and shaken vigorously for 30 min on a shaker at 4°C. After separating the organic and aqueous phase by centrifugation, the latter was taken up and frozen at -80°C until used. The extracts were then dried by speed-vac, redissolved in 15 µl of pyridine containing methoxamine (40 mg/ml) and incubated for 90 min at 30°C, under agitation. Finally, samples were derivatized with 30 µl of TMSFA at 37°C for 30 min and GC-MS analysis was performed as described in (6). dGSH was identified based on its retention time and characteristic ions. The selected ion monitoring chromatogram for m/z 398 was integrated using Masshunter software (Agilent) and areas were normalized to total ion current.

GC-MS-based analysis of urine from wild-type and *Nit1*-KO mice. The urine (50µl) from wild-type (n=7) and *Nit1*-KO (n=6) male mice were used for the metabolomics. Sample preparation and GC/MS measurement were the same as described (7). Urine was spiked with 100 nmol of D_3-creatine (Isotec, Miamisburg, OH) and treated with 30 units of type C-3 urease **(**Sigma-Aldrich**)** to remove interfering urea, after which urease was precipitated with ethanol and removed by centrifugation. The supernatant was then evaporated to dryness and the dried residue was treated with 100 µl of trimethylsilyl reagent, BSFTA (N,O-bis(trimethylsilyl)trifluoroacetamide)/TMCS (trimethylchlorosilane) (10:1) or *N,O*-Bis (trimethyl-d_9-silyl)acetamide and analyzed by low- or high-resolution GC-MS using a Hewlett-Packard GC-MSD.

Detection of 2-aminobutyrylglycine as product of the Nit1-catalyzed hydrolysis of dOA. dOA (120 µM) was incubated with 100 nM Nit1 in potassium phosphate buffer, pH 8 (0.42 ml total). After 30 min, the reaction was stopped by heating for 5 min at 80°C. A sample of the reaction mixture was treated with AQC, which afforded the labelling of compounds containing a primary amino group, and analyzed by HPLC on a reverse-phase column. The generation of a new amino compound in the reaction mixture, but not in a control where dOA had been omitted, was detected by the appearance of a new peak in the chromatogram. This chromatographic peak was collected and its identity with the AQC derivative of 2-aminobutyrylglycine was confirmed by both MS analysis and by comparison with a sample of authentic dipeptide treated with AQC.

Thiazolidine assay to detect cysteinylglycine. Release of cysteinylglycine from dGSH by Nit1 was measured spectrophotometrically through an assay in which the dipeptide was trapped in the form of a thiazolidine adduct with PLP. The principle of the assay is schematized in **Fig. S2A**. The reaction mixture (1 ml) contained 100 mM potassium phosphate buffer, pH 7.2, 0.5 mg/ml bovine serum albumin and 200 µM PLP. DTT was not included in these reactions, as it affected PLP absorption. The time-course of the reaction was followed at 388 nm.

Other transaminase assays. The transamination of glutamine (with production of α-KGM) by different aminotransferases was measured through a coupled assay with ω-amidase (scNit2) and GDH. The reaction mixture contained 50 mM Bicine buffer (pH 8.5), 50 mM KCl, 0.5 mg/ml bovine serum albumin, 2 mM DTT, ~0.22 mM NADH, 5 μM PLP, 5 mM ammonium acetate, 0.3 μM scNit2 and 2.4 units/ml GDH. All the transamination reactions leading to the production of α-KG were assayed through a coupled reaction with GDH. The OAT-catalyzed transamination of ornithine was measured through a coupled assay with pyrroline 5-carboxylate reductase from *E. coli* (expressed from an ASKA clone) (8).

Assessment of the activity of mmNit1 towards α-KG-CoA and other dicarboxylyl-CoAs. Different dicarboxylyl-CoAs, to be tested as potential substrates of mmNit1 (and, for comparison, also of mmNit2) were synthesized using recombinant human SUGCT (the product of a gene formerly termed *C7orf10*). The expression and purification of this enzyme have been described previously (9). For preparation of the dicarboxylyl-CoAs, the corresponding dicarboxylates (4 mM) were incubated at 30°C in a reaction mixture containing 50 mM potassium phosphate buffer at the desired pH (pH 7.0 in the case of α-KG; pH 7.5 in all other cases) as well as 0.1 mM glutaryl-CoA and 30 μg/ml SUGCT. The final volume of the reaction mixture was 50 μl. After incubation for a time sufficient to achieve the complete conversion of the glutaryl-CoA into the desired dicarboxylyl-CoA, mmNit1 or mmNit2 were added to the reaction mixture and incubation at 30°C was continued. Controls in which no amidase was added were run in parallel. Finally, the reaction was quenched by adding 150 μl of an ice-cold stop solution (5.4 M urea in the case of α-KG-CoA; 75 mM potassium phosphate, pH 4.5, for all other dicarboxylyl-CoAs); care was taken to ensure that, at the time of quenching, the consumption of substrate was still proceeding linearly. The resulting samples were kept on ice until analysis by reverse-phase HPLC, using a Varian 920-LC on a C18 column as described (9). The acyl-CoAs and the free CoA were detected and quantitated in the eluate by measuring the absorbance at 254 nm.

Subcellular localization of mmNit1. For studying the subcellular localization of mmNit1, the full length open reading frame of the mouse gene (either comprising or not the sequence coding for the first 38 amino acids, corresponding to the presumed mitochondrial propeptide) was PCR amplified and inserted in the pAcGFP1-N3 vector (Clontech) between the restriction sites NheI and EcoRI. This allowed for production of mmNit1 proteins in C-terminal fusion with GFP. Both constructs were transfected into CHO cells and the subcellular localization of the recombinant proteins was analyzed using confocal microscopy as previously described (9).

Methodology related to the genome analysis reported in Table S3. All homolog searches in complete genomes were performed by using the website of the Department of Energy, Integrated Microbial Genomes & Microbiomes (IMG/MER) (https://img.jgi.doe.gov/cgi-bin/mer/main.cgi).
Searches of Nit1/Nit2 homologs in complete genomes were performed by using the BLAST tool, in the 'Find genes' menu. Concatenated Nit1 proteins (mmNit1, mmNit2, ecYbeM, ecYaFV, paNit1, yeNit1, syNit1 and saYafV; 4 proteins at one time) were used for the homology searches. Among the sequences obtained by the BLAST searches, only those containing an Arg at position + 4 compared to the strictly conserved cysteine of the catalytic triad (Cys169 in scNit1) were taken into account, since this arginine binds the α-carboxylic group of α-KGM and dGSH. Percentage identity and scores were noted for all the alignments

that resulted from these searches. For a given sequence, assignment as ω-amidase or dGSH amidase was based on which functionally validated enzyme the sequence was most similar to. We also noted the identity of the residues that are most likely to play a major role in differentiating the dGSH/α-KGM specificity (as discussed in the main text). One of these residues is easy to trace, since it corresponds to residue +6 with respect to the strictly conserved glutamate in the catalytic triad. It is typically a small residue (Gly, Ala, Ser or Asp) in dGSH amidases and an aromatic residue (Phe, Tyr) in ω-amidases. The other residue is the one corresponding to Arg250 of scNit1 that interacts with the C-terminal carboxylic group of dGSH. It is typically a cationic residue (Arg or Lys) in dGSH amidases and a Phe or Tyr in ω-amidases. The assignment was noted as dubious if another residue was observed at these positions.

Searches of GSH synthetase homologs were performed similarly to that described above using concatenated eukaryotic synthetase/bacterial synthetase/bacterial bifunctional (γ-Glu-Cys synthetase/GSH synthetase) enzyme. The following sequences were used: *Mus musculus* (NP_032206.1) ; *Escherichia coli* (BAE77010.1); *Streptococcus thermophilus* WP_011226281. Percentage identity and scores were noted in the table for the alignment with the proteins that were identified. When a bifunctional protein was identified we checked carefully that the whole sequence aligned, rather than simply one of the two domains.

Searches of γ-Glu-Cys synthetase were similarly performed by using concatenated sequences corresponding of five widely different enzymes, in order to cover the whole spectrum of known γ-Glu-Cys synthetases (10). These sequences were derived from *Escherichia coli* (P0A6W9.1), *Mus musculus* (NP_034425.1), *Acidithiobacillus ferrooxidans* (WP_009561612.1), *Arabidopsis thaliana* (AAD14544.1) and *Synechocystis* sp. PCC 6803 (WP_010873241).
Note that the *E. coli* enzyme aligns with the γ-Glu-Cys synthetase portion of 'bifunctional' GSH synthetases.

SI APPENDIX - SUPPLEMENTARY TABLES

Table S1. Yeast strains used in this study

Name	Organism and Strain	Mutation
*yNit*2-KO	*S. cerevisiae* FY4	nit2::KanMX
*yNit*3-KO	*S. cerevisiae* FY4	nit3::KanMX

The wild-type strain used, *S. cerevisiae* FY4, is derived from S288C: *MATa SUC2 gal2 mal2 mel flo1 flo8-1 hap1 ho bio1 bio6*.

Table S2. Sequences of the primers used for PCR-mediated gene disruption in yeast, and for validation of yeast knockout strains

.

Primer	Sequence
ScNit2_Upstrm_F1	CCGGTACTGAACTTGTGTGC
ScNit2_Dwnstrm_R1	CGTACCATTAACAGAAAAGGCC
ScNit3_Upstrm_F2	GCTCGAACGCACAAATTG
ScNit3_Dwnstrm_R2	CGATGAGACTTTGTACACACCC
ISB_KanB_Rev	CTGCAGCGAGGAGCCGTAAT

Table S3. Occurrence of dGSH amidase, ω-amidase and GSH synthesizing enzymes in diverse organisms

	Species[a]	Putative dGSH amidase		Putative ω-amidase		γ-Glu-Cys synthetase[b]	GSH synthetase[c]	Thiol compound [d]
			DOE gene ID		DOE gene ID			
Col 1	Col2	Col3	Col4	Col5	Col6	Col7	Col8	Col9
Eukaryotes								
	Danio rerio	**mmNit1 55/341 Gly/Arg**	639482741	**mmNit2 78/466 Tyr/Tyr**	639480509	MusM 81/1078	Euk 64/597	
	Drosophila melanogaster	**mmNit1 50/282 Gly/Arg**	639550689	**mmNit2 51/310 Tyr/Tyr**	639553470	MusM 64/658	Euk 42/335	
	Saccharomyces cerevisiae	**mmNit1 38/208 Gly/Arg Tested**	638211686	**mmNit2 51/283 Tyr/Tyr Tested**	638212758	MusM 42/489	Euk 35/238	
	Arabidopsis thaliana	**mmNit1 45/259 Gly/Arg**	639575026	**mmNit2 57/218 Tyr/Tyr**	639579440	AraT 100/ 1084	Euk 39/292	
	Tetrahymena thermophila	**mmNit1 44/235 Ser/Arg**	2507590754	**mmNit2 47/252 Tyr/Tyr**	2507575332	MusM 41/264	Euk 32/196	
	Trypanosoma brucei	-	-	**mmNit2 45/246 Tyr/Tyr**	639627246	MusM 44/310	Euk 31/165	
	Eremothecium gossypii ATCC 10895	-	-	**mmNit2 48/258 Tyr/Tyr**	638223214	MusM 43/471	Euk 39/234	
	Plasmodium falciparum	-	-	-	-	MusM 37/150	Euk 28/99	
	Cryptosporidium parvum	-	-	-	-	None	None	
	Encephalitozoon intestinalis	-	-	-	-	None	None	
Bacteria								
Proteobacteria								
γ-proteobacteria								

Enterobacteriaceae	*Escherichia coli BL21*	**ecYbeM 99/483 Asp/Lys Tested**	6469117127	**ecYafV 99/539 Phe/Tyr Tested**	646916767	EscC 100/1008	Bac 100/662	GSH 27/7 µmol/g
	Enterobacter aerogenes EA1509	**ecYbeM 69/350 Ala/Arg**	2555653825	**ecYafV 83/463 Phe/Tyr**	2555654224	EscC 87/899	Bac 91/607	GSH 1.2 µmol/g
	Serratia marcescens B3R3	**yeNit1 79/473 Ala/Arg**	2688325862	**ecYafV 69/367 Phe/Tyr**	2688322039	EscC 77/772	Bac 82/546	GSH 0.2 µmol/g
	Yersinia enterocolitica 2516-87	**yaNit1 100/594 Ala/Arg Tested**	2638510043	**ecYafV 67/355 Phe/Tyr Tested**	2638509534	EscC 77/775	Bac 81/543	
	Yersinia pestis 1045	**yeNit1 91/539 Ala/Arg**	2637373883	-	-	EscC 76/471	Bac 80/538	
	Buchnera aphidicola 5A	-	-	-	-	EscC 50/507	Bac 63/445	
Aeromonadales	*Aeromonas hydrophila 4AK4*	**yeNit1 48/260 Gly/Arg**	2563671073	-	-	EscC 54/499	Bac 77/504	
		paNit1 45/202 Pro/Arg	2563672516	-	-			
Alteromonadales	*Shewanella baltica BA175*	**yeNit1 44/244 Gly/Arg**	648729849	-	-	EscC 53/454	Bac 72/481	
Pasteurellales	*Erwinia amylovora CFBP1430*	**ecYbeM 56/290 Asp/Arg**	646695637	**ecYafV 71/386 Phe/Tyr**	646695394	EscC 71/712	Bac 81/555	
	Actinobacillus succinogenes	-	-	-	-	(EscC 31/169)	Bif 47/653	
	Actinobacillus pleuropneumoniae	-	-	-	-	(EscC 29/144)	Bif 48/672	
	Haemophilus influenzae	-	-	-	-	None	None	GSH Import
	Pasteurella multocida	-	-	-	-	(EscC 30/151)	Bif 49/666	GSH Import

Pseudomonales	*Pseudomonas putida 1A00316*	**paNit1 79/413 Gly/Arg**	2689310231	**paYafV 51/245 Phe/Tyr**	2689310184	EscC 45/397	Bac 66/426	
	Pseudomonas aeruginosa 12-4-4 (59)	**paNit1 100/509 Gly/Arg Tested**	2687301550	**paYafV 49/250 Phe/Tyr Tested**	2689310184	EscC 46/384	Bac 65/424	
	Pseudomonas fluorescens A506	**paNit1 82/419 Gly/Arg**	2562288776	**paYafV 51/245 Phe/Tyr**	2562292272	EscC 44/381	Bac 67/432	GSH 1.6 µmol/g
	Azotobacter vinelandii CA	**paNit1 81/402 Gly/Arg**	2541769467	*YafV 49/243 Phe/His*	2541772210	EscC 47/402	Bac 65/421	GSH 8 µmol/g
	Acinetobacter calcoaceticus	**paNit1 43/194 Ala/Arg**	650426071	-	-	EscC 43/346	Bac 56/362	GSH 6 µmol/g
Vibrionales	*Vibrio alginolyticus Beneckea alginolytica*	**yeNit1 48/266 Gly/Arg**	2563757934	-	-	EscC 57/561	Bac 73/493	present
	Vibrio cholerae 2012EL-2176	**yeNit1 48/278 Gly/Arg**	2636899855	-	-	EscC 58/575	Bac 75/504	
	Vibrio fischeri MJ11 Photobacterium vibriofischeri	**yeNit1 46/260 Gly/Arg**	642779353	-	-	EscC 58/562	Bac 73/496	Present
	Vibrio natriegens NBRC 15636 Beneckea natriegens	**yeNit1 48/267 Ala/Arg**	2583690633	-	-	EscC 57/569	Bac 73/493	Present
Xanthomonadales	*Xanthomonas campestris 17*	-	-	**ecYafV 47/226 Phe/Tyr**	2642141327	AraT 59/555	Bac 56/357	
	Xanthomonas oryzae AXO 1947	-	-	**ecYafV 45/223 Phe/Tyr**	2674347981	AraT 59/552	Bac 56/358	
	Xylella fastidiosa 3214	-	-	**ecYafV 45/214 Phe/Tyr**	2510760755	AraT 57/526	Bac 53/333	

β-Proteobacteria								
Rhodocyclames	*Azoarcus sp BH72*	**paNit1 44/207 Ser/Arg**	639786432	-	-	AciF 56/454	Bac 48/288	
Burkholderales	*Alcaligenes faecalis*	**ecYbeM 52/273 Asn/Lys**	2630368615	-	-	EscC 43/374	Bac 47/303	GSH 25 µmol/g
		mmNit1 43/188 Gly/Met	2630367714	-	-			
	Bordetella avium	**ecYbeM 53/259 Asp/Arg**	641722553	-	-	EscC 44/368	Bac 45/268	
	Bordetella pertussis	**paNit1 46/198 Gly/Arg**	2632480223	-	-	None ??	Bac 47/293	
	Burkholderia cenocepacia	**paNit1 47/218 Gly/Arg**	2688602284			AciF 50/400	Bac 48/293	
Neisseriales	*Chromobacterium violaceum ATCC 12472*	**paNit1 48/205 Gly/Arg**	637452902	-	-	AciF 55/426	Bac 48/315	GSH 3 µmol/g
δ-Proteobacteria								
Desulfovibrionales	*Desulfovibrio vulgaris*	-	-	-	-	None	None	
Myxococcales	*Anaeromyxo-bacter dehalogenans*	**syNit1 49/256 Gly/Arg**	643596525	-	-	AraT 38/285	None	
Myxococcales	*Myxococcus xanthus DK 1622*	**syNit1 50/263 Ala/Arg**	638023440	-	-	AraT 39/287	Bac 39/224	GSH 0.8 µmol/g
	Sorangium cellulosum So Ce	**syNit1 50/234 Gly/Arg**	641348734			AraT 40/317	Bac 43/234	
	Stigmatella aurantiaca DW4/3-1	**syNit1 49/261 Gly/Arg**	649691109	-	-	AraT 37/280 AraT 32/234	Bac 42/240	
ε-Proteobacteria								
Campylobacterales	*Campylobacter jejuni*	-	-	-	-	None	None	

	Helicobacter pylori 2017					None	None	
α-Proteobacteria								
Rhizobiales	*Bradyrhizobium japonicum E109*	*yeNit1 41/207 Gln/Arg*				AraT 58/522	Bac 40/235	
Sphingomonadales	*Zymomonas mobilis mobilis ATCC 29191*	**ecYbeM 52/256 Asp/Arg**	2635565814			AraT 52/424	Bac 41/240	
Cyanobacteria								
Nostocales	*Anabaena variabilis*	**syNit1 73/429 Gly/Arg**	646570574			Syne 64/513	Bac 33/196	
Chroococclaes	*Synechocystis sp. GT-S, PCC 6803*	**syNit1 100/568 Gly/Arg Tested**	651080170			Syne 100/799	Bac 38/324	
Oscillatoriales	*Cyanothece sp. BH68*	**syNit1 75/444 Gly/Arg**	641674860			Syne 63/503	Bac 40/235	
Actinobacteria								
Actinomycetales	*Salinispora arenicola CNS-205*	**mmNit1 44/213 Gly/Arg**	641273299	-	-	AraT 27/106 Syne 23/72	None	
	Arthrobacter alpinus ERGS4 :06	*ecYbeM 37/153 Val/ ???*	2686646253	-	-	*Syne 24/66 AraT 23/72*	None	
	Corynebacterium glutamicum	-	-	*mNit2 31/144 Phe/Pro*	2653119440	*Syne 28/56*	None	
Bifidobacteriales	*Bifidobacterium longum (B)*	-	-	*ecYbeM 45/210 Arg/ Arg* **Tested**	2650840504	AraT 31/144	None	
	Streptomyces griseus griseus	-	-	*mmNit2 36/146 Ala/Gln*	6416998107	*AraT 29/98 Syne 23/57*	None	Mycothiol no GSH
	Streptomyces coelicolor A3(2)	-	-	*mmNit2 37/157 Ala/Phe*	637268060	*AraT 31/118*	None	
Micrococcales	*Micrococcus luteus*	*ecYbeM 38/148 Gly/Asp*	644805203	-	-	*Syne 24/59*	None	no GSH

Rubrobacterales	*Rubrobacter radiotolerans RSPS-4*	**syNit1 46/221 Gly/Arg**	2574650371			*Syne 27/77 Syne 24/47*	Unknown	GSH present
	Rubrobacter xylanophilus DSM9941	**syNit1 46/210 Gly/Arg**	638036051			*Syne 26/84 Syne 24/73 Syne 21/54*	Unknown	GSH present
Firmicutes								
Bacillales	*Bacillus amylo-liquefasciens B15*	-	-	**saYafV 40/199 Tyr/Phe**	2675096167	None	None	
	Bacillus subtilis 916	-	-	**saYafV 40/199 Tyr/Phe**	2638356656	None	None	Bacillithiol ; no GSH
	Bacillus thuringiensis HD-789	-	-	**saYafV 42/211 Tyr/Phe**	2518896022	None	None	
	Staphylococcus aureus 04-02981	-	-	**saYafV 100/546 Tyr/Tyr Tested**	646947436	None	None	GSH 0.5 µmol/g
	Staphylococcus epidermidis 949_S8	-	-	**saYafV 61/369 Tyr/Tyr**	2668331694	None	None	no GSH
Clostridia	*Clostridium botulinum 111*	-	-	**mmNit2 45/266 Tyr/Tyr**	2687274363	None	None	
	Clostridium kluyverii DSM 555	-	-	**mmNit2 50/285 Tyr/Tyr**	640858806	None	None	no GSH
	Clostridium pasteurianum	-	-	-	-	None	None	no GSH
	Clostridium perfringens	-	-	-	-		Bif 39/534	
Lactobacillales	*Enterococcus faecium*	-	-	-	-		Bif 49/721	
	Lactobacillus casei	-	-	-	-		Bif 27/136	GSH 0.8 µmol/g

	Lactobacillus plantarum 16	-	-	**saYafV 42/211 Tyr/Phe**	2563643469	EscC 30/119	Bif 28/311	
	Lactococcus lactis lactis = Streptococcus lactis					None	None	Import ? GSH 4.6 µmol/g
	Leuconostoc mesenteroides			**saYafV 38/191 Tyr/Phe**	2559087816	EscC 24/95	None	γ-GluCys
	Listeria monocytogenes			**saYafV 38/179 Tyr/Phe**	2575557058		Bif 41/550	
	Streptococcus agalactiae	-	-	-	-		Bif 63/982	GSH 3.2 µmol/g
	Streptococcus salivarius 57.I			**saYafV 42/209 Tyr/Phe**	651237238		Bif 94/1495	no GSH
	Streptococcus pneumoniae 70585					*AraT 22/63*	None	
Deinococcus-thermus								
Deinococcus	*Deinococcus radiodurans ATCC BAA-816*	-	-	-	-	None	None	
Thermus	*Thermus thermophilus HB27*	-	-	-	-	None	None	
Diderm								
Spirochaetales	*Borrelia burdorferi B31*	-	-	-	-	None	None	
	Treponema pallidum	-	-	-	-	None	None	
	Leptospira biflexa Patoc 1	**syNit1 47/261 Gly/Arg**	642688857	-	-	EC 37/287	Bif (partim) 41/228*	
	Brachyspira hyodysenteriae	-	-	-	-	None	None	

Acidobacteria								
	Acidobacterium capsulatum ATCC 51196	-	-	-	-	None	None	
	Terriglobus saanensis SP1PR4(T)	-	-	-	-	None	None	
	Chloracidobacterium thermophilum	-	-	-	-	None	None	
Aquificae								
	Aquifex aeolicus VF5	-	-	*ecNit1 29/104 Phe/Arg*	637019430	None	None	
Amatimonadetes								
	Chthonomonas calidirosea T49	-	-	-	-	None	None	
	Fimbriimonas ginsengisoli Gsoil 348	-	-	*ecYafV 31/100 Tyr/Phe*	2559127202	None	None	
Bacteroidetes								
	Bacteroides fragilis 638R	-	-	**ecYafV 44/224 Phe/Tyr**	650608259	None	None	
	Bacteroides thetaiotaomicron VPI-5482	-	-	**ecYafV 44/227 Phe/Tyr**	637408664	None	None	
	Cytophaga hutchinsonii ATCC 33406	-	-	**ecYafV 46/234 Phe/Tyr**	638070701	None	None	
Caldiserica								
	Caldisericum exile AZM16c01	-	-	-	-	None	None	
Chlamidiae								
	Chlamydia trachomatis A/363	-	-	-	-	None	None	

	Simkania negevensis Z	-	-	-	-		Bif 34/405	
Chlorobi								
	Chlorobium tepidum	-	-	-	-	None	None	
	Chlorobium phaeobacteroides BS1	-	-	-	-	None	None	
	Pelodictyon phaeoclathratiforme	-	-	-	-	None	None	
Chloroflexi								
	Chloroflexus aurantiacus J-10	-	-	-	-	None	None	
	Sphaerobacter thermophilus 4ac11	*mmNit1 47/188 Gly/Gly*	646435220	-	-	None	None	
Chrysiogenetes								
	Desulfurispirillum indicum S5, DSM 22839	-	-	*saYafV 32/130 Phe/Met*	649843077	EscC 38/324	Euk 33/192	
Deferribacteres								
	Denitrovibrio acetiphilus N2460	*YbeM 35/135 Arg/Gly*	646669419	*saYafV 28/118 Phe/Asp*	646669695	None	None	
	Deferribacter desulfuricans SSM1	-	-	*saYafV 29/113 Phe/Thr* *saYafV 30/98 Phe/Gly*	646662094 646662245	*Syne 35/62*	None	
Dictyoglomi								
	Dictyoglomus turgidum	-	-	-	-	None	None	

Elusimicrobia								
	Elusimicrobium minutum	-	-	-	-	None	None	
Fibrobacteres								
	Fibrobacter succinogenes S85	-	-	*ecYafV 34/123 Tyr/Leu*	650418148	None	None	
Fusobacteria								
	Fusobacterium nucleatum nucleatum ATCC 25586	-	-	-	-	None	None	
	Ilyobacter polytropus CuHBu1	-	-	*saYafV 37/136 Phe/Leu*	649701689		Bif 40/513	
Gemmatimonad-etes								
	Gemmatimonas aurantiaca	-	-	-	-	None	None	
Ignavibacteria								
	Melioribacter roseus P3M	-	-	*saYafV 34/140 Phe/Tyr*	2517206818	None	None	
Kryptonia								
	Kryptonium sp. JGI-2	-	-	-	-	None	None	
Nitrospirae								
	Leptospirillum ferriphilum ML-04	-	-	-	-	None	None	
	Nitrospira moscoviensis NSP M-1	-	-	-	-	None	None	

Planctomycetes								
	Pirellula sp. SH-Sr6A	-	-	-	-	None	None	
	Phycisphaera mikurensis	-	-	-	-	None	None	
Synergistetes								
	Thermanaerovibrio acidaminovorans Su883	-	-	*saYafV 33/139 Tyr/Asp*	646434111	None	None	
	Anaerobaculum mobile NGA	-	-	*saYafV 35/167 Tyr/Lys*	2509690846	None	None	
Mollicutes								
	Acholeplasma laidlawii	-	-	-	-	None	None	
	Mycoplasma pneumonia 19294	-	-	-	-	None	None	
Thermodesulfo-bacteria								
	Thermodesulfobacterium commune	-	-	-	-	None	None	
Thermotogae								
	Thermotoga maritima MSB8	-	-	-	-	None	None	
	Fervidobacterium nodosum	-	-	-	-	None	None	
Verrucomicrobiae								
	Akkermansia muciniphila	-	-	-	-	None	None	
	Opitutus terrae	-	-	-	-	None	None	

Archaea								
Euryarchaeota								
	Archaeoglobus fulgidus			**mmNit2 33/131 Phe/Tyr**	2588653119	None	None	
Halobacteriales								
	Haloarcula marismortui ATCC 43049			*mmNit2 34/144 Tyr/Glu*	638182507	Sy 31/67	None	
	Natrialba magadii			*mmNit2 40/221 Gly/Val*	646647639	Sy 30/56	None	
	Haloferax mediterranei ATCC33500			*mmNit2 41/214 Gly/Glu*	2578424449	Sy 29/57	None	
	Haloferax volcanii DS2 ATCC29605			*mmNit2 41/206 Gly/Val*	646698619	Sy 28/58		γ–GluCys
Methanobacteriales								
	Methanobacterium formicicum BRM9			**mmNit2 54/327 Tyr/Tyr**	2631417720	None	None	
	Methanobrevibacter ruminantium M1			**mmNit2 46/288 Tyr/Tyr**	646531679	EC 34/167	None	

This Table was assembled to assess whether enzymes that are highly likely (or proven) to be dGSH amidases co-occur with the enzymes for the biosynthesis of GSH in a series of organisms. Each genome was searched for homologs of γ-glutamyl cysteine synthetase, GSH synthetase and amidases, as described in the Methods section in Supplementary Information. For dGSH amidase and ω-amidase (columns 3 and 5), the indicated protein (see nomenclature in Table 1 of the main text) is the one showing the highest percentage identity/highest score out of the eight tested proteins (see Methods). The identities of the two amino acids deemed to be important for determining the dGSH amidase/ω–amidase specificity are also indicated (see multiple alignments in **Fig. S14A**). For **ω-amidase**, the presence of Tyr or Phe at both of these positions is considered as confirming the assignment (**bold** types are then used); substitution by another residue leads to dubious assignment (*italicized* types are then used). For **dGSH amidase** we used as a criterion for assignment the following combination of criteria: (1) identity > 38 % and score > 180 for

the comparison with an amidase showing higher activity with dGSH than with α-KGM; (2) the presence of Gly, Ala, Ser, Asp or Asn as the first 'specificity' residue; (3) the presence of Arg or Lys as second specificity residue. **Bold** types are used if all these criteria are met and *italics* if not. Columns 4 and 6 indicate the gene identification number in the DOE website.

[a] Species have been highlighted with the following color code: (yellow) presence of GSH synthetase and dGSH amidase (n = 38); (cyan) absence of GSH synthetase but presence of dGSH amidase (n = 2); (red) presence of GSH synthetase but absence of dGSH amidases (n =19); (green) absence of both (n = 62); (grey) dubious cases due to uncertain assignment of a potential amidase (n = 13).
[b]The figures indicate the percentage identity and score for the alignment with γ-glutamyl cysteine synthetases from *Acidothiobacillus ferrooxidans* (AciF), *Arabidopsis thaliana* (AraT), *Escherichia coli* (EscC), *Mus musculus* (MusM), and *Synechocystis* sp. PCC 6803 (Syne).
[c]The figures indicate the percentage identity with γ-glutamyl cysteine synthetases from a eukaryote (Euk; *Mus musculus*), a bacterium (Bac, *Escherichia coli*) or the bifunctional enzyme (Bif) of *Streptococcus thermophilus*. Note that *Rubrobacter* sp. contains still another, unknown form of GSH synthetase (11).
[d]Direct evidence for the presence or absence of GSH in bacteria is based on the literature, particularly on the works of Fahey (10, 12).

SI APPENDIX - SUPPLEMENTARY FIGURES

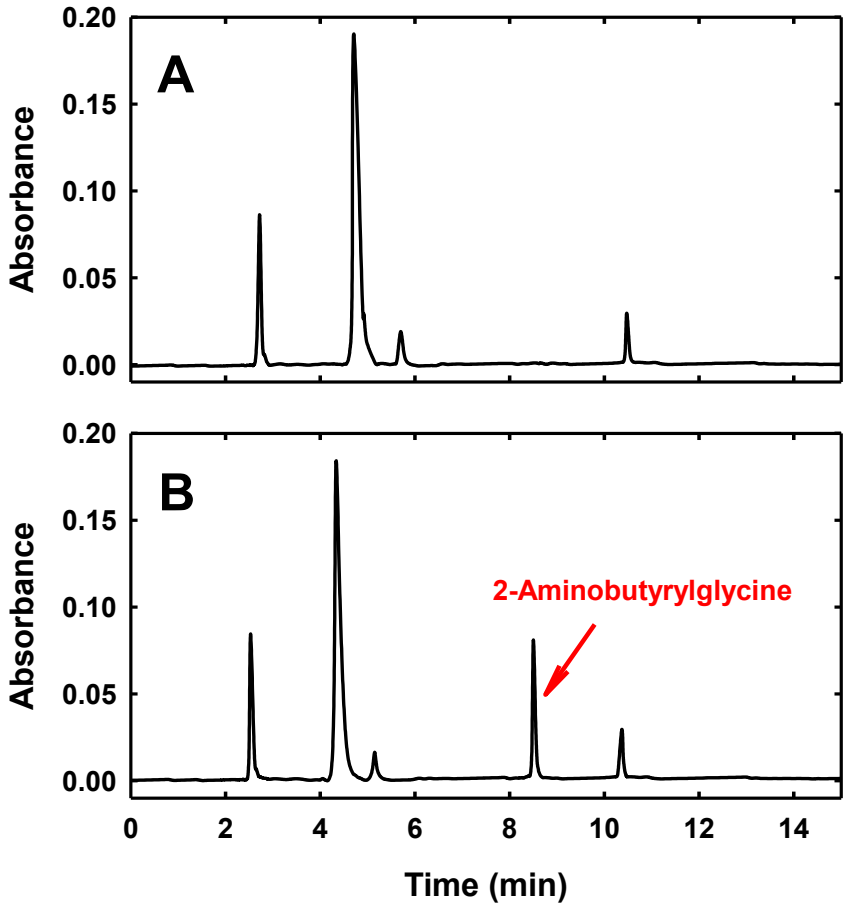

Fig. S1. Identification of the second product made from dOA by Nit1. (A) Control, in which a solution of dOA (120 μM) in 50 mM potassium phosphate buffer, pH 8 was incubated for 30 min at 30°C, then heated for 5 min at 80°C and finally derivatized with 6-aminoquinolyl-N-hydroxysuccinimidyl carbamate (AQC), before being analyzed by HPLC on a reverse-phase column. Analytes were detected based on their absorbance at 358 nm. None of the peaks in the chromatogram corresponds to dOA (which lacks a primary amino group). (B) In this case, the incubation of dOA was conducted in the presence of 100 nM mmNit1. The new peak in the chromatogram was shown to correspond to 2-aminobutyrylglycine (the expected product of the Nit1 reaction) by both MS analysis and by comparison with a sample of authentic 2-aminobutyrylglycine treated with AQC.

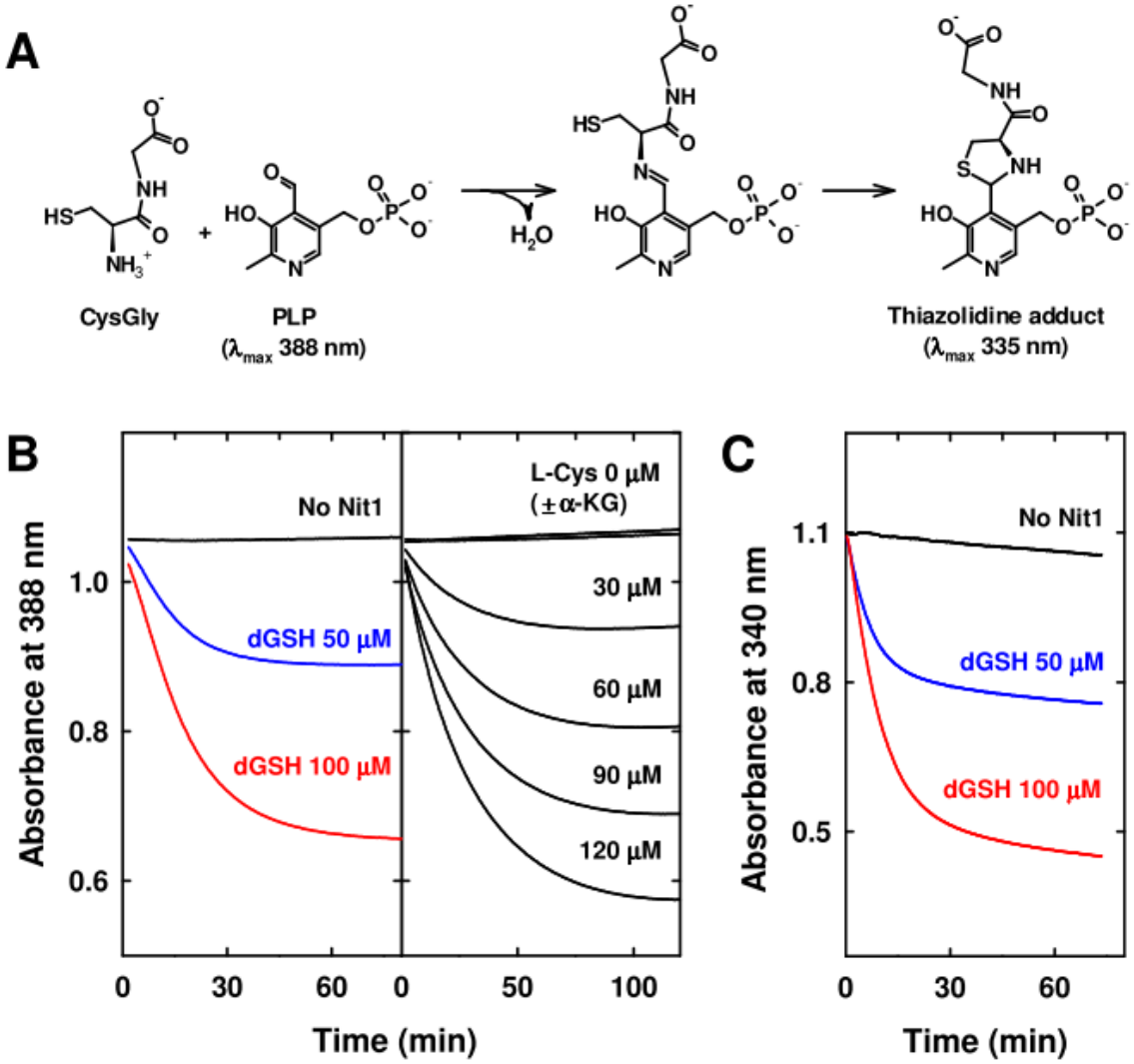

Fig. S2. Release of cysteinylglycine in the Nit1 reaction, monitored through formation of a thiazolidine adduct. (A) Principle of the assay. Contrary to dGSH, which lacks a primary amino group, cysteinylglycine can bind to pyridoxal 5'-phosphate (PLP) via formation of a Schiff base. This is followed by attack of the thio group on the imine carbon, to form a thiazolidine adduct with greatly decreased absorption at 388 nm (13, 14). (B) Reactions of mmNit1 (100 nM) with 0, 50 or 100 µM dGSH, performed in the presence of 200 µM PLP (100 mM potassium phosphate buffer, pH 7.2, 30°C) and monitored at 388 nm. To appreciate the quantitative response of the assay, the overall decreases in absorption due to the Nit1 reactions (left panel), are compared with the decreases observed upon direct addition of different concentrations of L-cysteine to the PLP solution (right panel). [The reaction of L-cysteine with PLP is slightly slower than that with cysteinylglycine at pH 7.2 (13), but results in a thiazolidine adduct whose absorption properties are essentially identical to those of the species formed by cysteinylglycine]. (C) Reactions of mmNit1 (100 nM) with 0, 50 or 100 µM dGSH, monitored through the coupled assay with GDH (which detects the release of α-KG). Reaction conditions were the same as in panel B, except that PLP was replaced by 200 µM NADH, 5 mM ammonium acetate and 2.4 units GDH.

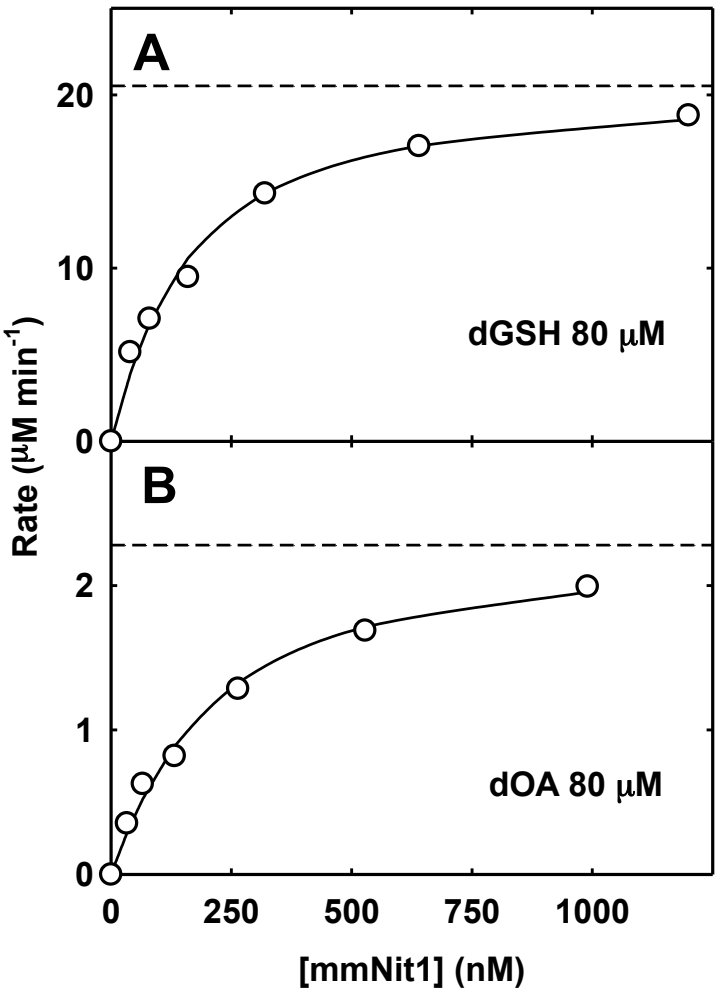

Fig. S3. Rate of spontaneous opening of the cyclic dGSH and dOA forms at pH 7.2. (A) The observed rate of dGSH hydrolysis is plotted as a function of increasing mouse Nit1 concentrations (50 mM Hepes-K, pH 7.2). The concentration of dGSH was 80 μM. The leveling off of the reaction rate indicates that, at high mmNit1 concentrations, the overall process is rate-limited by opening of the cyclic form of dGSH. The dashed line represents the asymptote for the observed rate (20.5 μM min^{-1}) which, divided by the dGSH concentration, yields the apparent first-order rate constant for ring opening (0.26 min^{-1}). The same first-order constant was obtained when using the yeast Nit1 ortholog (scNit1) and/or when performing the experiment at different dGSH concentrations. At the same pH, opening of the cyclized α-KGM occurs 240-fold more slowly (apparent first-order rate constant of 0.0011 min^{-1}: (15)), suggesting the occurrence of some type of intramolecular catalysis in dGSH. (B) Same as above, except that dOA (80 μM) was used instead of dGSH. In this case, the asymptote was much lower, and the calculated rate constant for dOA opening was 0.029 min^{-1}. This implies that the presence of the thiol group in dGSH contributes substantially to increasing the ring opening rate.

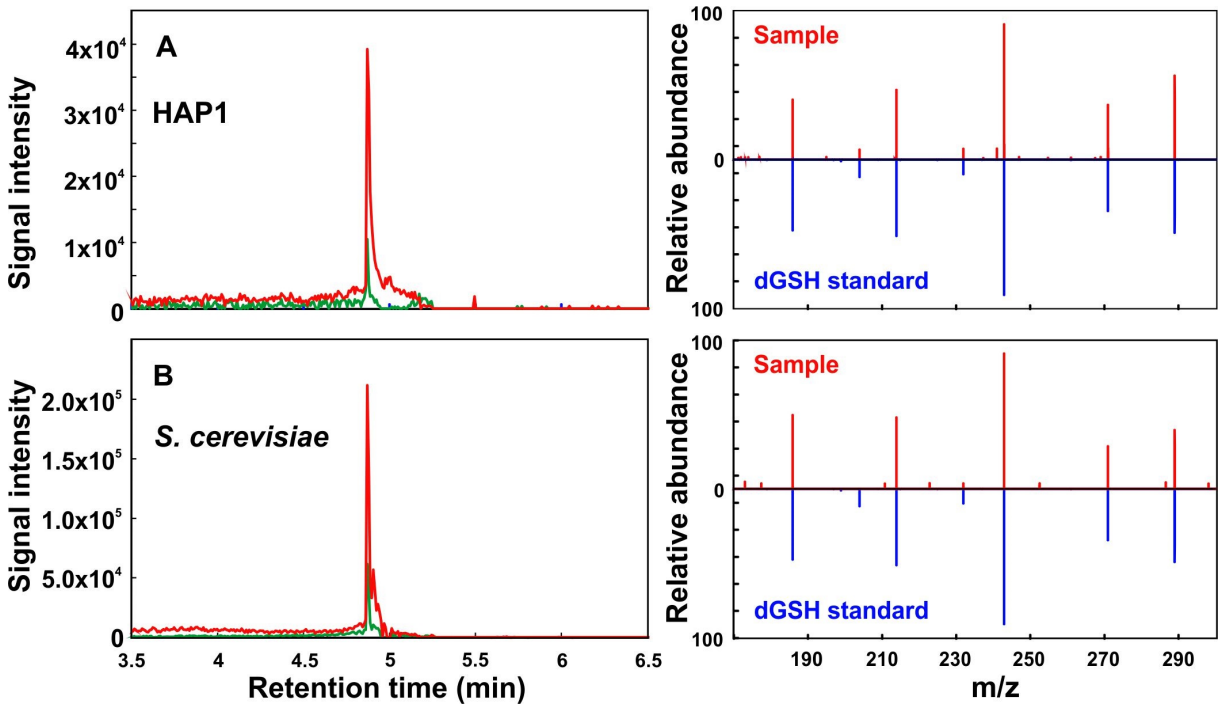

Fig. S4. LC-MS evidence for the accumulation of dGSH in samples from Nit1-deficient cell models. (A) Extracted ion chromatogram overlays (*m/z* 307.058-307.061) are shown for *Nit1*-KO (red line) and WT (green line) extracts from HAP1 cells. The panel on the right shows the MS2 spectrum of dGSH found in the Nit1-deficient samples mirrored with the MS2 spectrum generated from a standard of purified dGSH. (B) Same as above, but for extracts of *S. cerevisiae*. The green line represents the chromatogram for WT yeast extract. The red line is the chromatogram for the yeast strain lacking the Nit1 ortholog (scNit1, see Table 1 of the main text).

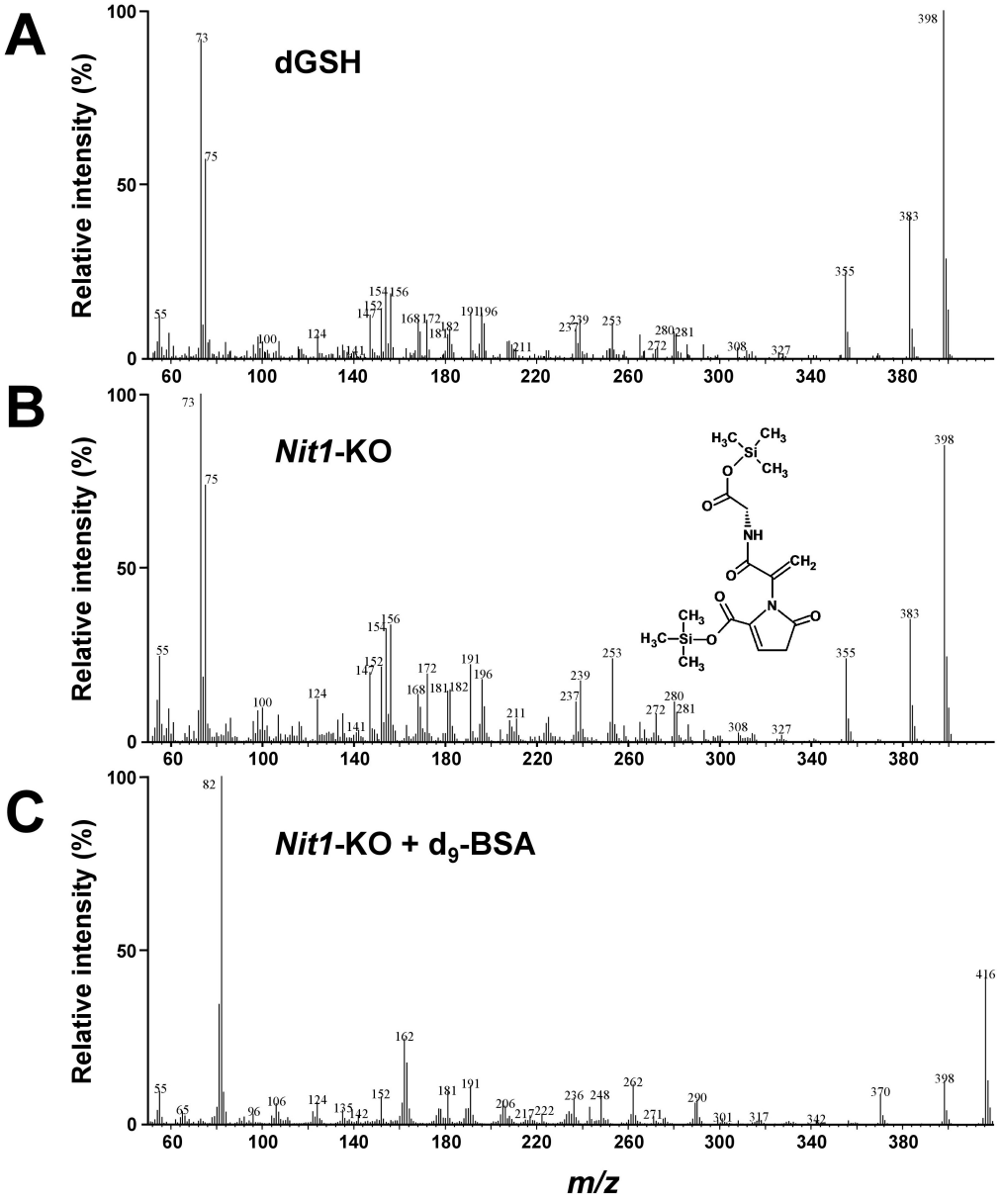

Fig. S5. Mass spectra of the compound with retention time 11.97 min obtained in GC-MS analysis of purified dGSH or of the urine of *Nit1*-KO mice. (A) Mass spectrum of the compound with retention time 11.97 min observed in the GC/MS chromatogram of purified dGSH (peak shown in Fig. 4C of the main text). (B) Mass spectrum of the same compound from the urine of *Nit1*-KO mice. This is a replica of Fig. 4D in the main text. The inset shows the structure for the dGSH derivative. (C) Mass spectrum of the compound (retention time 11.97 min) observed when the urine of *Nit1*-KO mice was silylated with *N,O*-Bis (trimethyl-d_9-silyl)acetamide (d_9-BSA). The shift of the molecular ion from *m/z* 398 to *m/z* 416 implies that the compound contains two trimethylsilyl moieties.

Fig. S6. GC-MS chromatograms of extracts from *Nit1*-KO, *Nit2*-KO and wild-type HAP-1 cell lines collected in the single ion mode (SIM; *m/z* 398) allowing the detection of a specific dGSH derivative in Nit1 deficient cells – A distinctive peak eluting at 35.3 min is detected in Nit1-KO cells with SIM at *m/z* 398. The same specific derivative of dGSH (molecular ion at *m/z* 398) is better detected by GC-MS in the urine of *Nit1*-KO mice (where dGSH is very concentrated) and is shown in Fig. 4 of the main text together with its spectrum. Note that the GC-MS apparatus/column for this analysis was completely different from the one used in Fig. 4 of the main text, so the distinctive peak for the dGSH derivative elutes with a different retention time. The identity of this peak was confirmed in control experiments, in which wild-type cell extracts were spiked with purified dGSH.

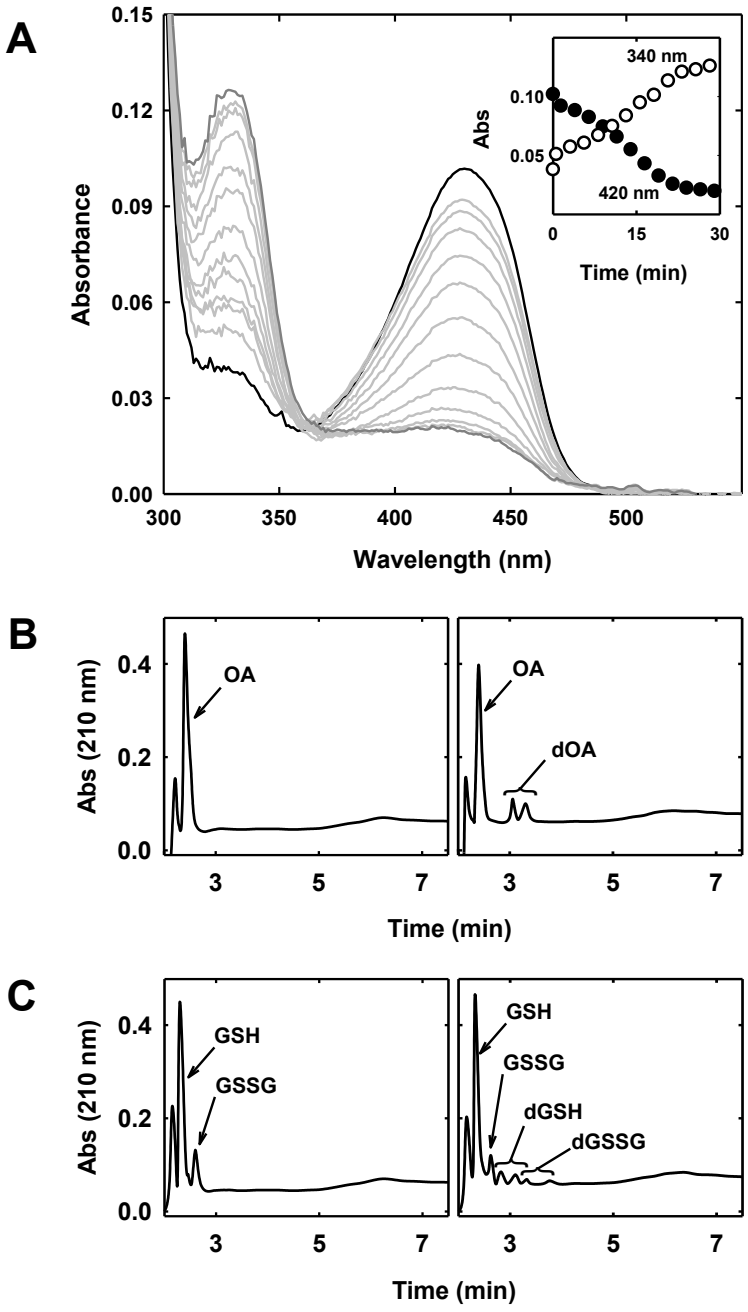

Fig. S7. Transamination of GSH and OA by recombinant human glutamine transaminase K (KYAT1). (A) Time-dependent spectral changes during the reaction of the enzyme (20 μM) with 5 mM GSH in 50 mM Bicine-K buffer, pH 8.5. Prior to adding GSH, the transaminase had been reacted with a stoichiometric amount of glyoxylate, to convert any trace of bound pyridoxamine 5'-phosphate (PMP) into pyridoxal 5'-phosphate (PLP). The PLP spectrum, with a main band at 430 nm, did not appreciably decrease for at least one hour in the absence of GSH. (B) HPLC chromatogram of reaction mixtures in which OA (10 mM) and glyoxylate (5 mM) were incubated for 16 hr in the absence (left) or in the presence (right) of 4 μM KYAT1. The two new peaks in the right panel were identified as dOA (two anomers) based on MS/MS data (see Fig. S8) (C) HPLC chromatograms of reaction mixtures in which GSH (10 mM) and glyoxylate (5 mM) had been incubated for 5 hr in the absence (left) or in the presence (right) of 4 μM KYAT1. GSSG denotes a glutathione disulfide (oxidized GSH); dGSSG indicates mixed disulfides of the two isomers of dGSH with GSH. Identities of the peaks in the right panel were established by MS/MS analysis (see Fig. S9).

A

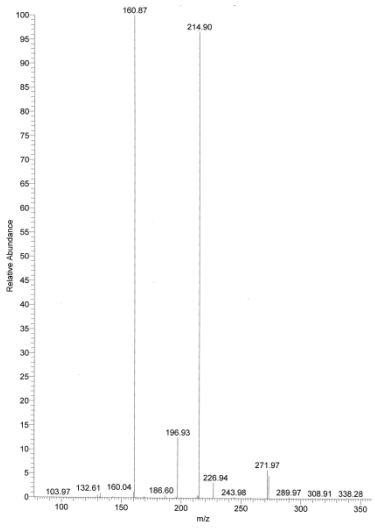

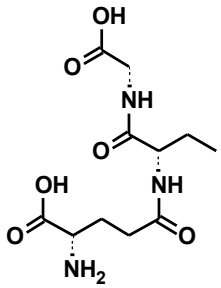

Fragments (proposed)
290 = M +H
272 = M +H – H_2O
227 = M +H – H_2O – HCO_2
215 = M +H – Gly
197 = 215 – H_2O
161 = M +H – Gln

B

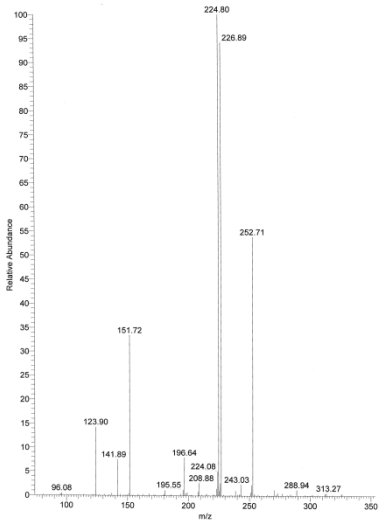

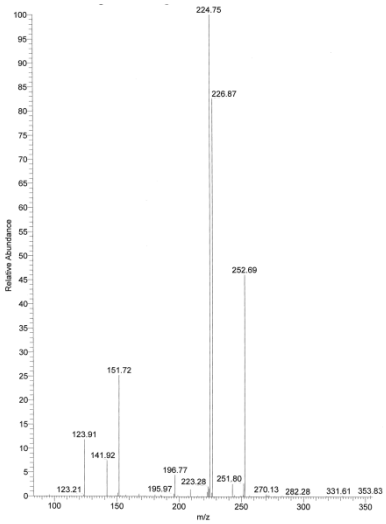

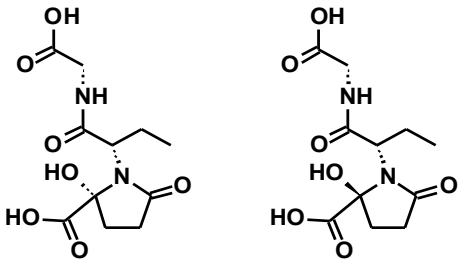

Fragments (proposed)
289 = M +H
271 = M +H – H_2O
253 = M +H – H_2O – H_2O
227 = M +H – H_2O – CO_2
225 = M +H – H_2O – H_2CO_2
151 = M +H – H_2O – CO2 – Gly

Fig. S8. Mass spectra of the peaks for reagents and products in Fig. S7B. (A) Peak labelled OA from Fig. S7B - Ophthalmic acid (reaction reagent): MS/MS of m/z 290 $(M + H)^+$. (B) Peaks labelled dOA from Fig. S7B. Both correspond to deaminated ophthalmic acid (reaction product present in the cyclized (lactam) form): MS/MS of m/z 289 $(M + H)^+$.

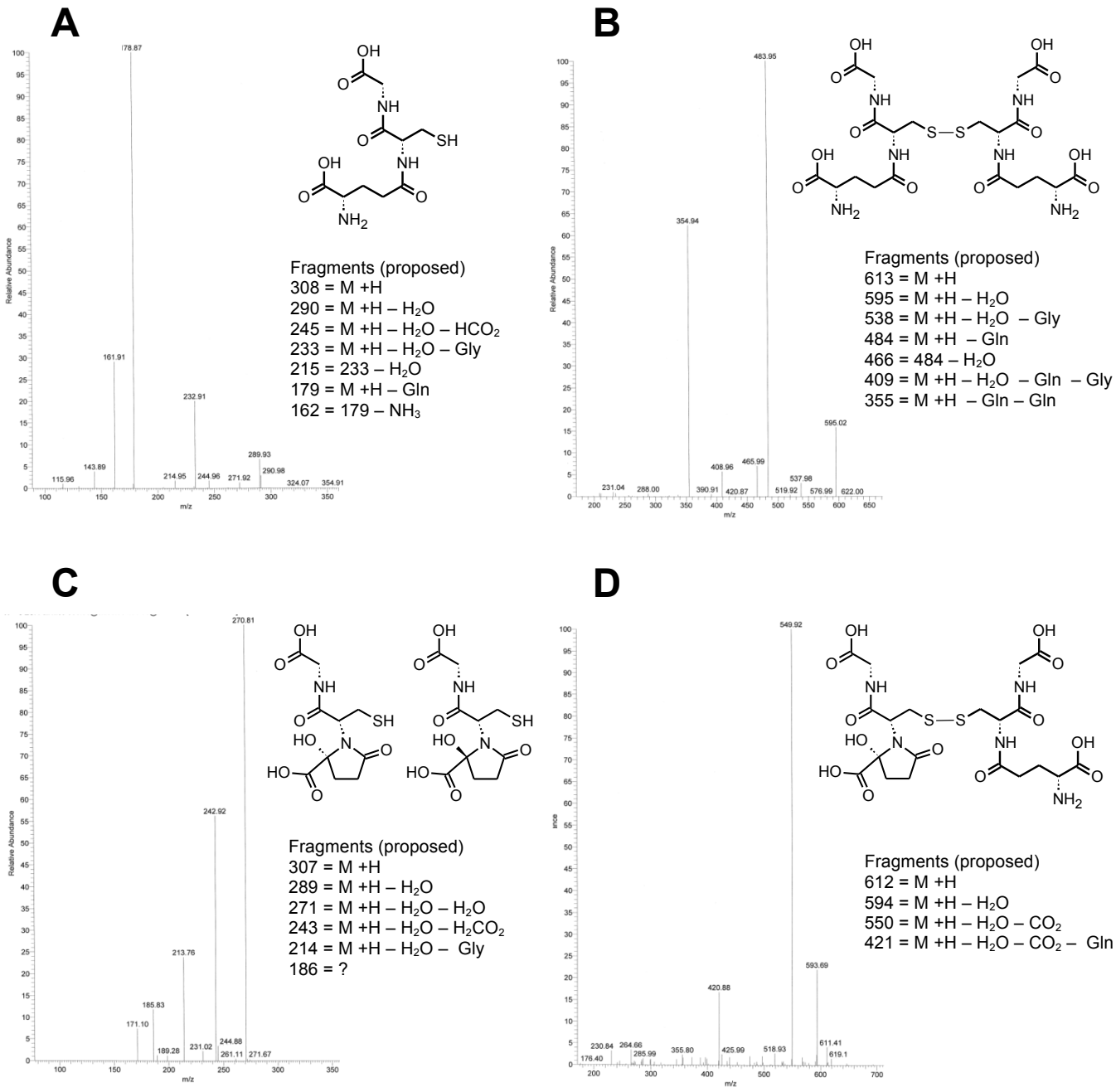

Fig. S9. Mass spectra of the peaks for reagents and products from Fig. S7C. (A) Peak labelled GSH in Fig. S7C (reduced glutathione; substrate of the reaction): MS/MS of *m/z* 308 $(M + H)^+$. (B) Peak labelled GSSG (oxidized glutathione) in Fig. S7C. MS/MS of *m/z* 613 $(M + H)^+$. (C) One of the two peaks labelled dGSH (deaminated glutathione, occurring in two different anomeric forms). MS/MS of *m/z* 307 $(M + H)^+$. The other peak showed an essentially identical mass spectrum. (D) One of the peaks labelled dGSSG (mixed disulfide of glutathione and deaminated glutathione, only the structure of one anomeric form is shown for simplicity). MS/MS of *m/z* 612 $(M + H)^+$. The other peak showed a mass spectrum essentially identical to the one presented here.

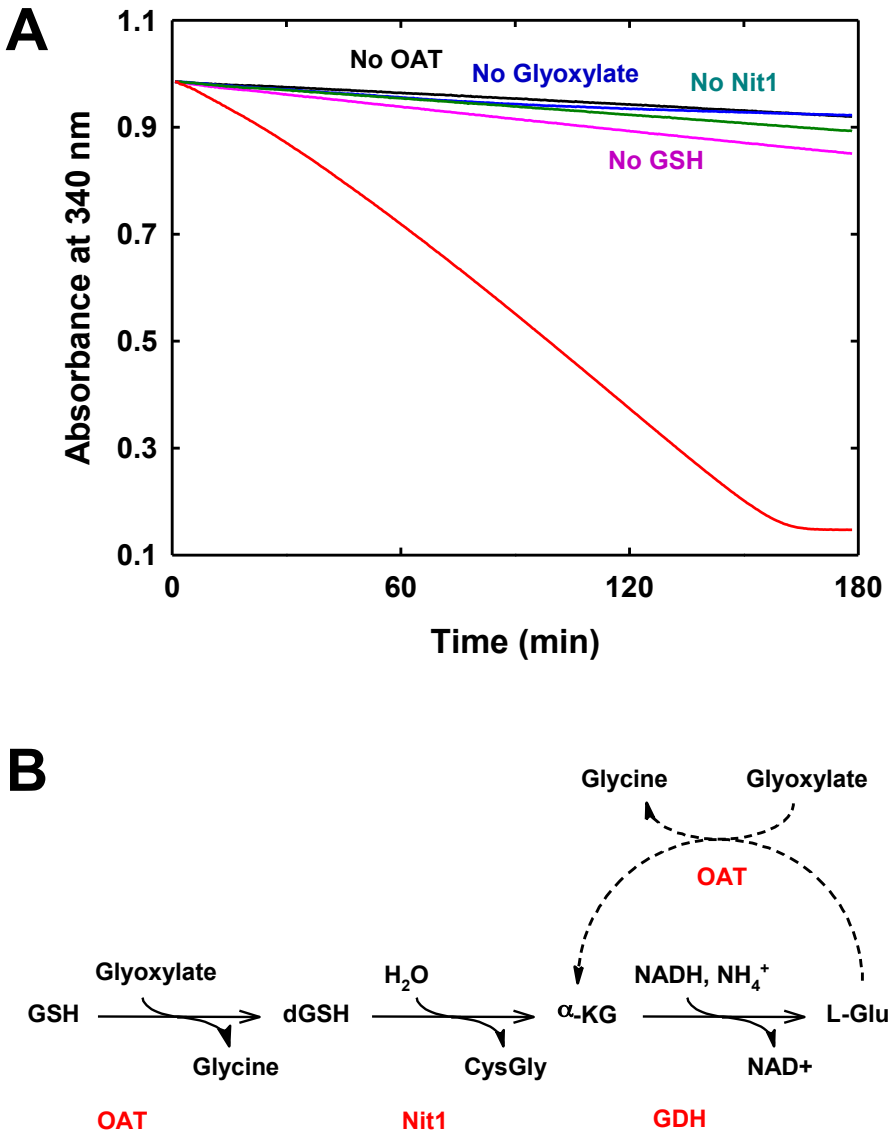

Fig. S10. An example of continuous spectrophotometric assay, monitoring dGSH production by recombinant mouse ornithine aminotransferase (OAT). (A) GDH activity (reflecting the release of α-KG in the reaction mixture) was detected upon addition of OAT (1.2 μM), and only if the mixture contained GSH, glyoxylate and Nit1. Omission of any of these reagents almost prevented the decrease in absorbance at 340 nm due to oxidation of NADH. The complete reaction mixture (red curve) contained 15 mM GSH, 3 mM glyoxylate and 1.2 μM OAT (50 mM Bicine-K buffer, pH 8.5). Note that the GDH reaction seemed to accelerate progressively with time. As explained in panel (B), this was likely due to the fact that the glutamate generated by GDH was being reconverted by OAT to α-KG, which in turn could serve again as a GDH substrate, promoting an artefactual amplification of the signal.

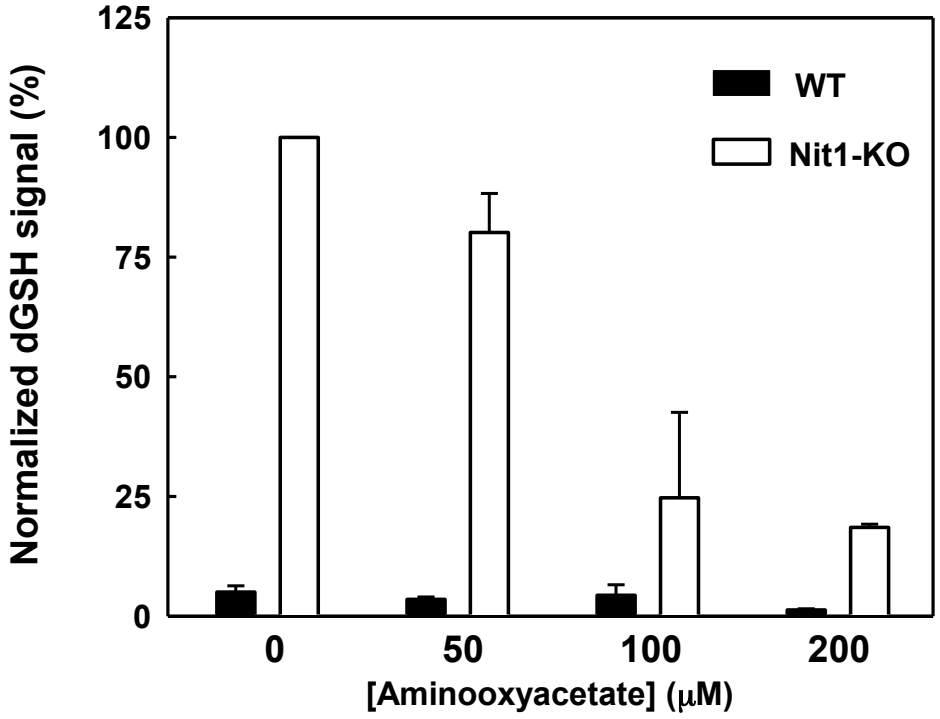

Fig. S11. Inhibition of transaminases by aminooxyacetate (AOA) substantially decreases dGSH accumulation in *Nit1*-KO cells. 10^6 HAP1 cells, both wild-type (WT1) and *Nit1*-KO (Nit1-T1; see Fig. 2 of the main text), were seeded in 6-cm plates containing 6 ml of media supplemented with different amounts of AOA. After 24h, cells were extracted with methanol and the extract was analyzed by GC-MS. The intensity of the dGSH peak (*m/z* 398 species; see Fig. 4 of the main text and Fig. S6) was normalized with respect to the signal corresponding to the total ion current, to correct for the decrease in cell mass observed in the presence of AOA. The reported values (averages of three replicates ± SEM) are expressed as % of the intensity of the dGSH peak in the untreated *Nit1*-KO cells.

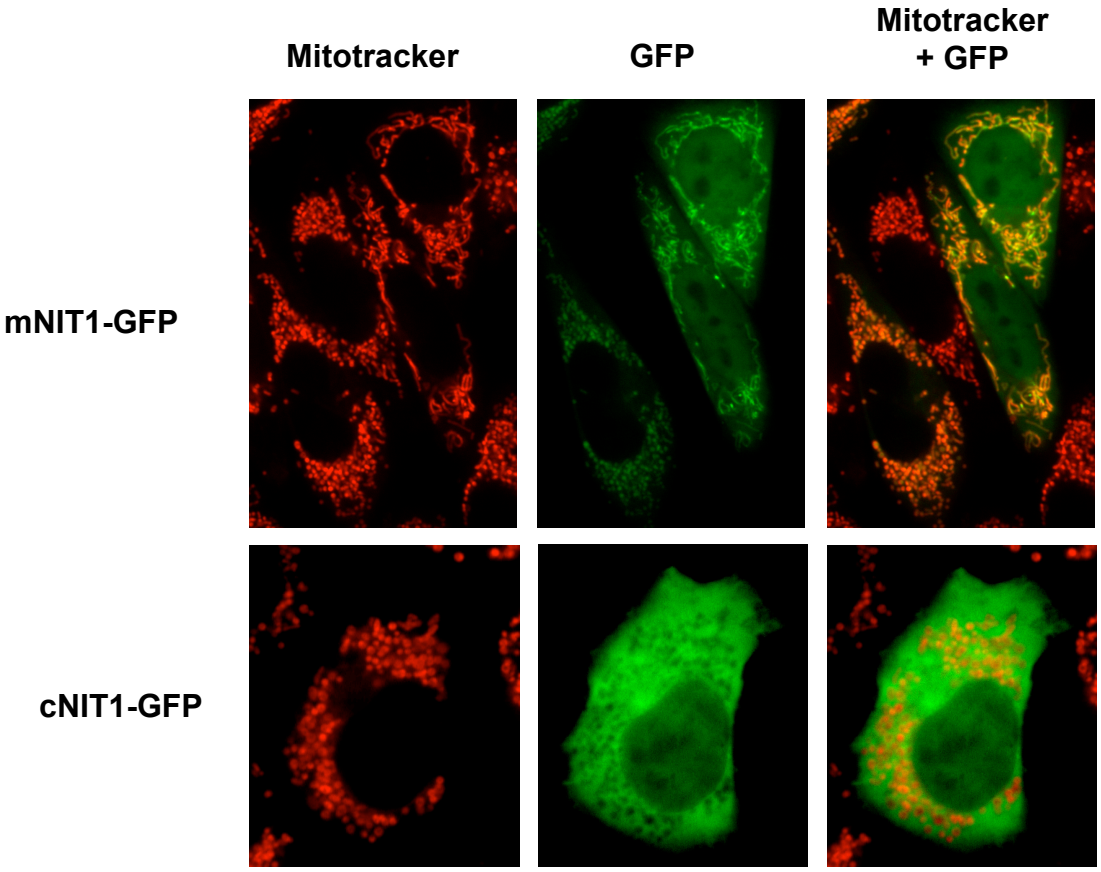

Fig. S12. Subcellular localization of the Nit1 protein. CHO cells were transfected with plasmid pAcGFP1-N3, containing the coding sequence for the mouse Nit1 fused to GFP. In the mNit1-GFP construct, the mouse Nit1 retained the mitochondrial localization signal, whereas in the cNit1-GFP construct the signal peptide was removed. Cells were incubated for 24 hours at 37°C before labelling with Mitotracker (Thermo Fisher) for 20 min, and subsequently analyzed by fluorescence microscopy as described (9), with excitation wavelengths of 480 nm (GFP) and 561 nm (Mitotracker).

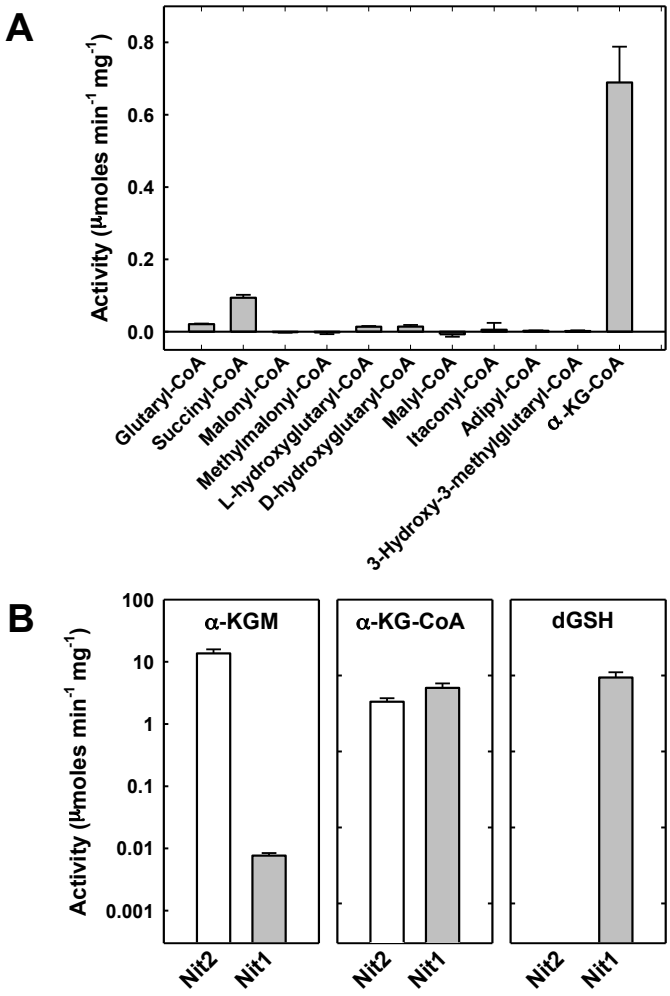

Fig. S13. Activity of mouse Nit1 towards α-KG-CoA. (A) Rate of mmNit1-catalyzed CoA release from a number of dicarboxylyl-CoA derivatives. The experiments were conducted as described in the Methods. (B) Comparison of the hydrolase activity of mmNit1 and mmNit2 towards different substrates (note the logarithmic scale on the y-axis). The results shown are averages (± SEM) of at least three separate measurements. In the case of dGSH, mmNit2 activity was essentially undetectable ($\leq 3\times10^{-4}$ μmoles·min^{-1}·mg^{-1}; Table 2 in the main text). Data within the same panel are directly comparable, but data between panels are not, for several reasons. First, the assay conditions differed depending on the substrate (α-KGM hydrolysis by mmNit1 and mmNit2 was tested using 0.4 mM α-KGM in 50 mM Bicine-K buffer, pH 8.5, 30°C; reactions with α-KG-CoA were carried out using ~100 μM substrate in 50 mM potassium phosphate, pH 7.0, 30°C; while dGSH hydrolysis was measured using 80 μM substrate in 50 mM Bicine-K buffer, pH 8.5, 30°C). Second, the hydrolysis of α-KG-CoA involves a thioester bond, rather than a much more stable amide linkage. Finally, α-KGM and dGSH exist predominantly in an unreactive cyclic form, whereas α-KG-CoA does not cyclize. The similar activities of mmNit1 and mmNit2 towards α-KG-CoA imply that the CoA moiety of this substrate presumably does not fit in the same part of the Nit1 catalytic pocket that hosts the cysteinylglycine moiety of dGSH. A distinct binding mode of the substrate might be allowed by the higher flexibility of the thioester bond in α-KG-CoA as compared to the amide bond of dGSH. In any event, the fact that mmNit1 and mmNit2 display similar activities towards α-KG-CoA, but drastically different activities towards dGSH, suggests that the evolutionary pressure allowing the conservation of Nit1 is based on its capacity to hydrolyze dGSH.

A

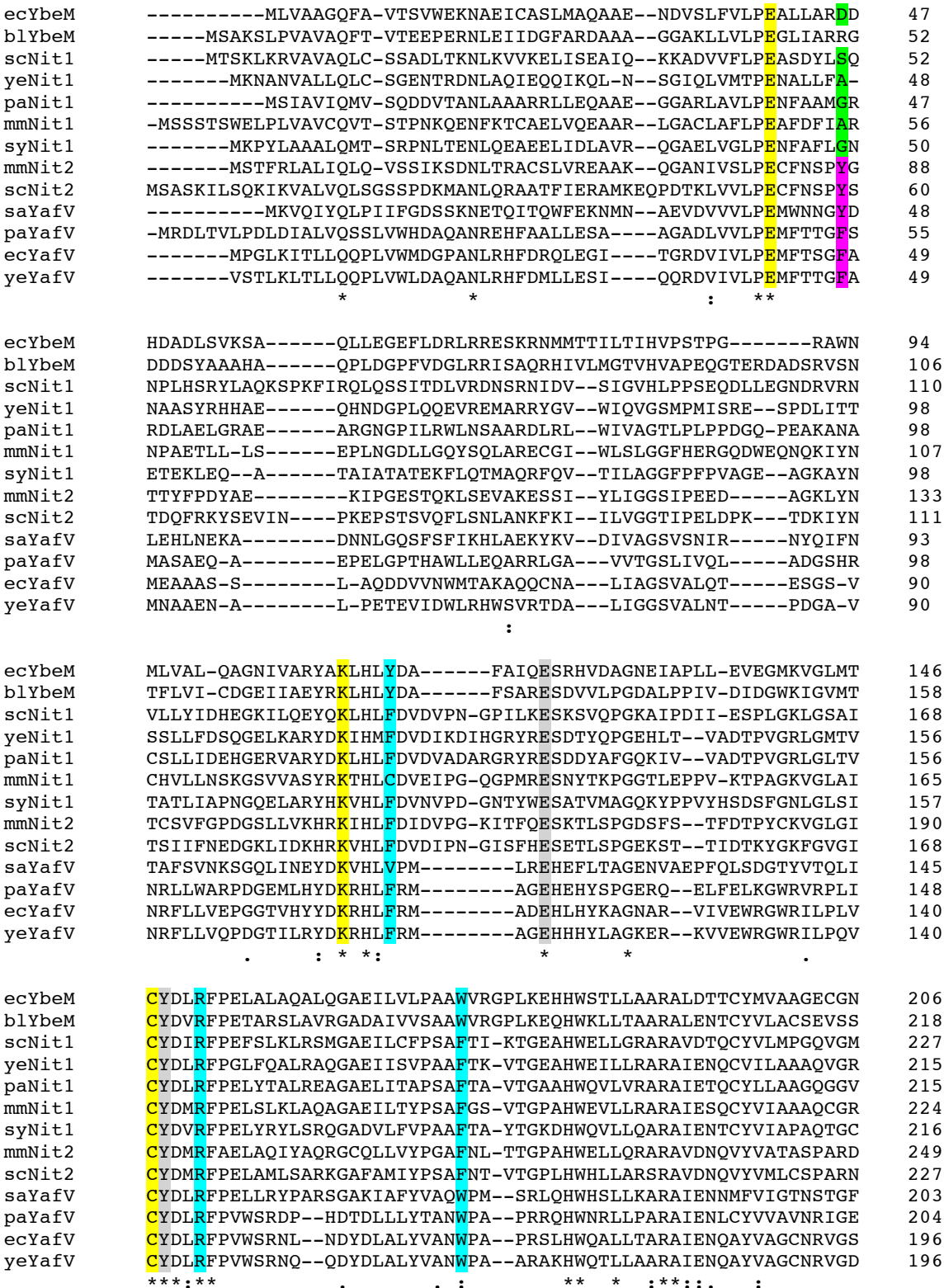
ecYbeM ----------MLVAAGQFA-VTSVWEKNAEICASLMAQAAE--NDVSLFVLPEALLARDD 47
blYbeM -----MSAKSLPVAVAQFT-VTEEPERNLEIIDGFARDAAA--GGAKLLVLPEGLIARRG 52
scNit1 -----MTSKLKRVAVAQLC-SSADLTKNLKVVKELISEAIQ--KKADVVFLPEASDYLSQ 52
yeNit1 -------MKNANVALLQLC-SGENTRDNLAQIEQQIKQL-N--SGIQLVMTPENALLFA- 48
paNit1 ----------MSIAVIQMV-SQDDVTANLAAARRLLEQAAE--GGARLAVLPENFAAMGR 47
mmNit1 -MSSSTSWELPLVAVCQVT-STPNKQENFKTCAELVQEAAR--LGACLAFLPEAFDFIAR 56
syNit1 -------MKPYLAAALQMT-SRPNLTENLQEAEELIDLAVR--QGAELVGLPENFAFLGN 50
mmNit2 -------MSTFRLALIQLQ-VSSIKSDNLTRACSLVREAAK--QGANIVSLPECFNSPYG 88
scNit2 MSASKILSQKIKVALVQLSGSSPDKMANLQRAATFIERAMKEQPDTKLVVLPECFNSPYS 60
saYafV ----------MKVQIYQLPIIFGDSSKNETQITQWFEKNMN--AEVDVVVLPEMWNNGYD 48
paYafV -MRDLTVLPDLDIALVQSSLVWHDAQANREHFAALLESA----AGADLVVLPEMFTTGFS 55
ecYafV -------MPGLKITLLQQPLVWMDGPANLRHFDRQLEGI----TGRDVIVLPEMFTSGFA 49
yeYafV -------VSTLKLTLLQQPLVWLDAQANLRHFDMLLESI----QQRDVIVLPEMFTTGFA 49
ecYbeM HDADLSVKSA------QLLEGEFLDRLRRESKRNMMTTILTIHVPSTPG-------RAWN 94
blYbeM DDDSYAAAHA------QPLDGPFVDGLRRISAQRHIVLMGTVHVAPEQGTERDADSRVSN 106
scNit1 NPLHSRYLAQKSPKFIRQLQSSITDLVRDNSRNIDV--SIGVHLPPSEQDLLEGNDRVRN 110
yeNit1 NAASYRHHAE------QHNDGPLQQEVREMARRYGV--WIQVGSMPMISRE--SPDLITT 98
paNit1 RDLAELGRAE------ARGNGPILRWLNSAARDLRL--WIVAGTLPLPPDGQ-PEAKANA 98
mmNit1 NPAETLL-LS------EPLNGDLLGQYSQLARECGI--WLSLGGFHERGQDWEQNQKIYN 107
syNit1 ETEKLEQ--A------TAIATATEKFLQTMAQRFQV--TILAGGFPFPVAGE--AGKAYN 98
mmNit2 TTYFPDYAE--------KIPGESTQKLSEVAKESSI--YLIGGSIPEED-----AGKLYN 133
scNit2 TDQFRKYSEVIN----PKEPSTSVQFLSNLANKFKI--ILVGGTIPELDPK---TDKIYN 111
saYafV LEHLNEKA--------DNNLGQSFSFIKHLAEKYKV--DIVAGSVSNIR-----NYQIFN 93
paYafV MASAEQ-A--------EPELGPTHAWLLEQARRLGA---VVTGSLIVQL-----ADGSHR 98
ecYafV MEAAAS-S--------L-AQDDVVNWMTAKAQQCNA---LIAGSVALQT-----ESGS-V 90
yeYafV MNAAEN-A--------L-PETEVIDWLRHWSVRTDA---LIGGSVALNT-----PDGA-V 90
ecYbeM MLVAL-QAGNIVARYAKLHLYDA------FAIQESRHVDAGNEIAPLL-EVEGMKVGLMT 146
blYbeM TFLVI-CDGEIIAEYRKLHLYDA------FSARESDVVLPGDALPPIV-DIDGWKIGVMT 158
scNit1 VLLYIDHEGKILQEYQKLHLFDVDVPN-GPILKESKSVQPGKAIPDII-ESPLGKLGSAI 168
yeNit1 SSLLFDSQGELKARYDKIHMFDVDIKDIHGRYRESDTYQPGEHLT--VADTPVGRLGMTV 156
paNit1 CSLLIDEHGERVARYDKLHLFDVDVADARGRYRESDDYAFGQKIV--VADTPVGRLGLTV 156
mmNit1 CHVLLNSKGSVVASYRKTHLCDVEIPG-QGPMRESNYTKPGGTLEPPV-KTPAGKVGLAI 165
syNit1 TATLIAPNGQELARYHKVHLFDVNVPD-GNTYWESATVMAGQKYPPVYHSDSFGNLGLSI 157
mmNit2 TCSVFGPDGSLLVKHRKIHLFDIDVPG-KITFQESKTLSPGDSFS--TFDTPYCKVGLGI 190
scNit2 TSIIFNEDGKLIDKHRKVHLFDVDIPN-GISFHESETLSPGEKST--TIDTKYGKFGVGI 168
saYafV TAFSVNKSGQLINEYDKVHLVPM--------LREHEFLTAGENVAEPFQLSDGTYVTQLI 145
paYafV NRLLWARPDGEMLHYDKRHLFRM--------AGEHEHYSPGERQ--ELFELKGWRVRPLI 148
ecYafV NRFLLVEPGGTVHYYDKRHLFRM--------ADEHLHYKAGNAR--VIVEWRGWRILPLV 140
yeYafV NRFLLVQPDGTILRYDKRHLFRM--------AGEHHHYLAGKER--KVVEWRGWRILPQV 140
ecYbeM CYDLRFPELALAQALQGAEILVLPAAWVRGPLKEHHWSTLLAARALDTTCYMVAAGECGN 206
blYbeM CYDVRFPETARSLAVRGADAIVVSAAWVRGPLKEQHWKLLTAARALENTCYVLACSEVSS 218
scNit1 CYDIRFPEFSLKLRSMGAEILCFPSAFTI-KTGEAHWELLGRARAVDTQCYVLMPGQVGM 227
yeNit1 CYDLRFPGLFQALRAQGAEIISVPAAFTK-VTGEAHWEILLRARAIENQCVILAAAQVGR 215
paNit1 CYDLRFPELYTALREAGAELITAPSAFTA-VTGAAHWQVLVRARAIETQCYLLAAGQGGV 215
mmNit1 CYDMRFPELSLKLAQAGAEILTYPSAFGS-VTGPAHWEVLLRARAIESQCYVIAAAQCGR 224
syNit1 CYDVRFPELYRYLSRQGADVLFVPAAFTA-YTGKDHWQVLLQARAIENTCYVIAPAQTGC 216
mmNit2 CYDMRFAELAQIYAQRGCQLLVYPGAFNL-TTGPAHWELLQRARAVDNQVYVATASPARD 249
scNit2 CYDMRFPELAMLSARKGAFAMIYPSAFNT-VTGPLHWHLLARSRAVDNQVYVMLCSPARN 227
saYafV CYDLRFPELLRYPARSGAKIAFYVAQWPM--SRLQHWHSLLKARAIENNMFVIGTNSTGF 203
paYafV CYDLRFPVWSRDP--HDTDLLLYTANWPA--PRRQHWNRLLPARAIENLCYVVAVNRIGE 204
ecYafV CYDLRFPVWSRNL--NDYDLALYVANWPA--PRSLHWQALLTARAIENQAYVAGCNRVGS 196
yeYafV CYDLRFPVWSRNQ--QDYDLALYVANWPA--ARAKHWQTLLAARAIENQAYVAGCNRVGD 196

```
ecYbeM      ----------------------KNIGQSRIIDPFGVTIAAAS---EMPALIMAEVTPER    240
blYbeM      ----------------------RNIGCCRIIDPMGEVVAEAG--DEGAELIATGLSREC    253
scNit1      HDLSDPEWEKQSHMSALEKSSRRESWGHSMVIDPWGKIIAHADPSTVGPQLILADLDREL    287
yeNit1      HG------------------ATRRTWGHTMAVDAWGKIIGQNP---DAVSALKVKIETTG    254
paNit1      HP------------------RGRETFGHSAIVDPWGRVLAERP---QGEAVLLAVRDAAE    254
mmNit1      HH------------------ETRASYGHSMVVDPWGTVVARCS---EGPGLCLARIDLHF    263
syNit1      HY------------------ERRHTHGHAMIIDPWGVILADAG---EKPGLAIAEINPDR    255
mmNit2      DK------------------ASYVAWGHSTVVDPWGQVLTKAG---TEETILYSDIDLKK    288
scNit2      LQ------------------SSYHAYGHSIVVDPRGKIVAEAG---EGEEIIYAELDPEV    266
saYafV      DG------------------N-TEYAGHSIVINPNGDLVGELN--E-SADILTVDLNLNE    241
paYafV      DG------------------NALRYAGDSQVLDFQGDSLFNAA--D-ADGVFRVRLDAAA    243
ecYafV      DG------------------NGCHYRGDSRVINPQGEIIATAD--AHQATRIDAELSMAA    236
yeYafV      DD------------------NGHHYQGNSVILDALGEIQAQAE--PGQAAQLDAELSLET    236
                                   *    ::  *

ecYbmE      VRQVRAQLPVLNNRRFAPPQLL----------      262
blYbeM      LASARQIMPVLQNRRFADPQLPD---------      276
scNit1      LQEIRNKMPLWNQRRDDLFH------------      307
yeNit1      LKTIRNQMPVLQHNRFVSSLVPRLSDSKQSSK      286
paNit1      QADIRRRMPVVAHRRFFPPAEPRPARTE----      282
mmNit1      LQQMRQHLPVFQHRRPDLYGSLGHPLS-----      290
syNit1      LKQVRQQMPSLQHRVFV---------------      272
mmNit2      LAEIRQQIPILKQKRADLYTVESKKP------      314
scNit2      IESFRQAVPLTKQRRFDVYSDVNAH-------      291
saYafV      VEQQRENIPVFKSIKLDLYK------------      261
paYafV      LAAYRQRFPAYMDADRFEIHP-----------      264
ecYafV      LREYREKFPAWQDADEFRLW------------      256
yeYafV      LQAYRERFPAFHDTDKFLLL------------      256
                *  .*
```

B

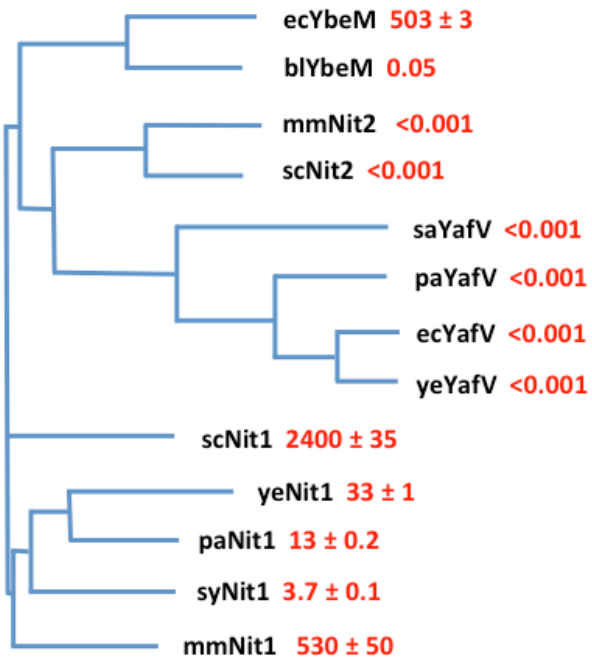

Fig. S14. (A) Multiple alignment of the thirteen Nit1/Nit2 homologs that were investigated in the present work. The residues of the 'catalytic triad' (Glu-Lys-Cys), conserved in all amidases, are shaded in yellow. Other residues that interact with the α-ketoglutaryl moiety of the substrate are shaded in cyan. Two additional, highly conserved residues are highlighted in light grey. Residues that are discussed in the text as potential discriminants between dGSH amidases and ω-amidases are shaded in green and magenta, respectively. Numbering of residues in *M. musculus* Nit2 is as in the crystal structure (16). (B) Phylogenetic tree derived from the alignment showing in red the ratio of dGSH amidase/ω-amidase activity (taken from Table 4 in the main text).

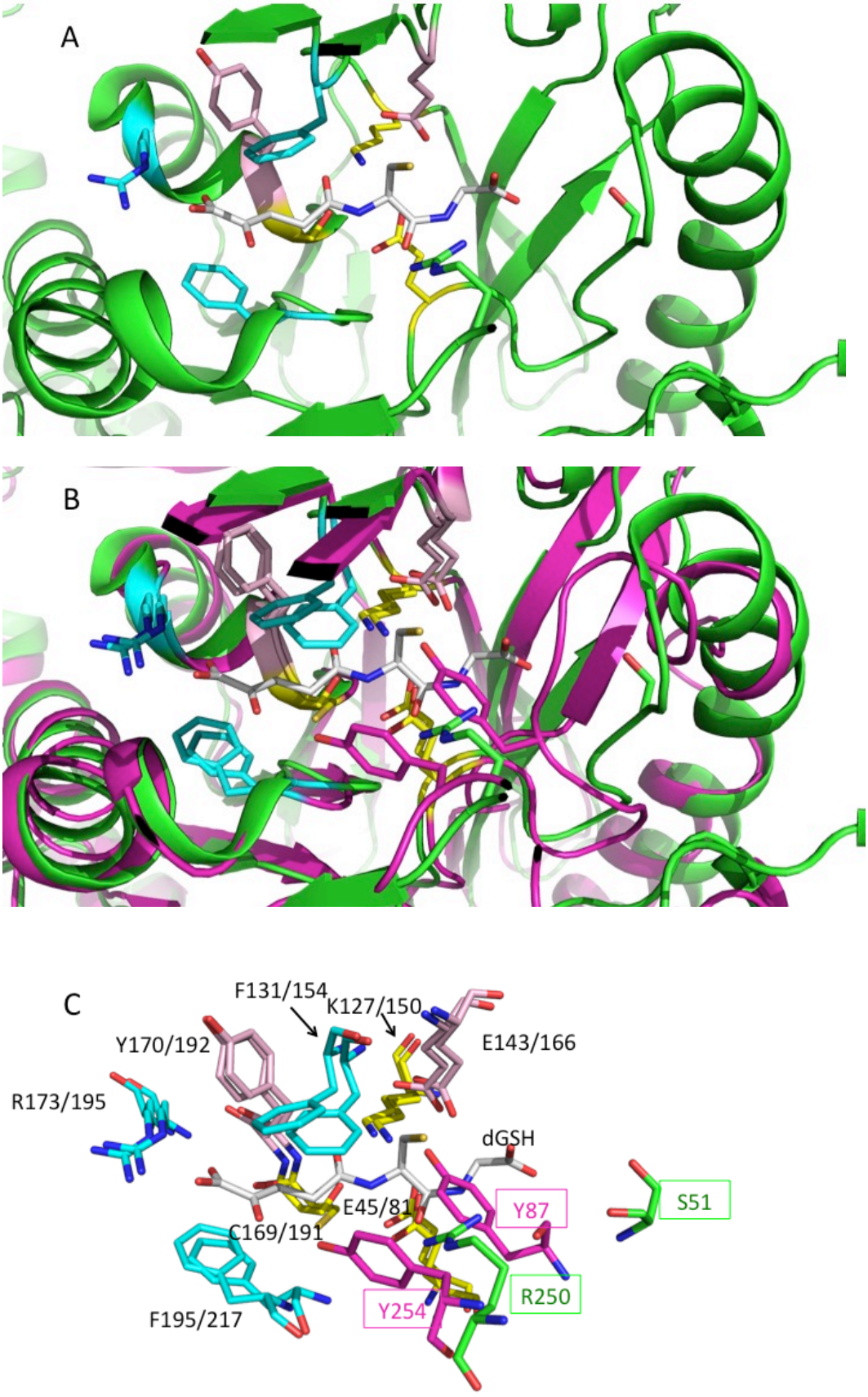

Fig. S15. Structure of the catalytic sites of the *S. cerevisiae* Nit1 ortholog (scNit1) and *M. musculus* Nit2 (mmNit2) showing the location of residues involved in substrate specificity. See legend on the following page.

Fig. S15. Structure of the catalytic sites of the *S. cerevisiae* Nit1 ortholog (scNit1) and *M. musculus* Nit2 (mmNit2) showing the location of residues involved in substrate specificity. (A) Structure of scNit1 (in green; pdb 4HGD (16)) with the putative dGSH molecule (in grey). The catalytic cysteine (Cys169) has been replaced by a serine in the crystallized protein (16), but is nonetheless designated as Cys169. (B) and (C) Superimposition of the same structure with *M. musculus* Nit2 (in magenta; pdb 2W1V (17)). These two structures were superimposed with a rmsd of 1.52Å. Residues are color-coded in the same way as in the alignment shown in Fig. S14A and their identity is shown in panel C. The residues of the catalytic triad (yellow), those that bind the α-ketoglutaryl moiety (cyan) and two additional highly conserved residues (light pink; Glu143, Tyr170 in scNit1; Glu166 and Tyr192 in mmNit2; light grey in Fig. S14A) are identically localized in the two structures. By contrast, the large 'subpocket' that accommodates the cysteinylglycine moiety of dGSH in scNit1 is occluded by the two 'ω-amidase diagnostic residues' Tyr87 and Tyr254 (magenta) in mmNit2, thus preventing the fixation of dGSH. One of the 'dGSH-amidase signature residues' (Arg250; green) of scNit1 interacts through its side chain with the carboxyl-end of dGSH while the other (Ser51; green) is small and at a distance from dGSH. The figure was drawn with PyMOL.

SI APPENDIX - SUPPLEMENTARY REFERENCES

1. Brachmann CB*, et al.* (1998) Designer deletion strains derived from *Saccharomyces cerevisiae* S288C: a useful set of strains and plasmids for PCR-mediated gene disruption and other applications. *Yeast* **14**(2)**:** 115-132.
2. Becker-Kettern J*, et al.* (2016) *Saccharomyces cerevisiae* forms D-2-hydroxyglutarate and couples its degradation to D-lactate formation *via* a cytosolic transhydrogenase. *J Biol Chem* **291**(12)**:** 6036-6058.
3. Semba S*, et al.* (2006) Biological functions of mammalian Nit1, the counterpart of the invertebrate NitFhit Rosetta stone protein, a possible tumor suppressor. *J Biol Chem* **281**(38)**:** 28244-28253.
4. Kurien BT, Scofield RH (1999) Mouse urine collection using clear plastic wrap. *Lab Anim* **33**(1)**:** 83-86.
5. Ran FA*, et al.* (2013) Genome engineering using the CRISPR-Cas9 system. *Nat Protoc* **8**(11)**:** 2281-2308.
6. Collard F*, et al.* (2016) A conserved phosphatase destroys toxic glycolytic side products in mammals and yeast. *Nat Chem Biol* **12**(8)**:** 601-607.
7. Kuhara T (2001) Diagnosis of inborn errors of metabolism using filter paper urine, urease treatment, isotope dilution and gas chromatography-mass spectrometry. *J Chromatogr B Biomed Sci Appl* **758**(1)**:** 3-25.
8. Juncosa JI, Lee H, Silverman RB (2013) Two continuous coupled assays for ornithine-δ-aminotransferase. *Anal Biochem* **440**(2)**:** 145-149.
9. Marlaire S, Van Schaftingen E, Veiga-da-Cunha M (2014) C7orf10 encodes succinate-hydroxymethylglutarate CoA-transferase, the enzyme that converts glutarate to glutaryl-CoA. *J Inherit Metab Dis* **37**(1)**:** 13-19.
10. Fahey RC (2013) Glutathione analogs in prokaryotes. *Biochim Biophys Acta* **1830**(5)**:** 3182-3198.
11. Johnson T, Newton GL, Fahey RC, Rawat M (2009) Unusual production of glutathione in Actinobacteria. *Arch Microbiol* **191**(1)**:** 89-93.
12. Fahey RC, Brown WC, Adams WB, Worsham MB (1978) Occurrence of glutathione in bacteria. *J Bacteriol* **133**(3)**:** 1126-1129.
13. Buell MV, Hansen RE (1960) Reaction of pyridoxal-5-phosphate with aminothiols. *J Am Chem Soc* **82**(6042-6049.
14. Schonbeck ND, Skalski M, Shafer JA (1975) Reactions of pyridoxal 5'-phosphate, 6-aminocaproic acid, cysteine, and penicilamine. Models for reactions of Schiff base linkages in pyridoxal 5'-phosphate-requiring enymes. *J Biol Chem* **250**(14)**:** 5343-5351.
15. Hersh LB (1971) Rat liver ω-amidase. Purification and properties. *Biochemistry* **10**(15)**:** 2884-2891.
16. Liu H*, et al.* (2013) Structures of enzyme-intermediate complexes of yeast Nit2: insights into its catalytic mechanism and different substrate specificity compared with mammalian Nit2. *Acta Crystallogr D Biol Crystallogr* **69**(Pt 8)**:** 1470-1481.
17. Barglow KT*, et al.* (2008) Functional proteomic and structural insights into molecular recognition in the nitrilase family enzymes. *Biochemistry* **47**(51)**:** 13514-13523.